Complex ceramic structures. I. Weberites

Lu Cai and Juan C. Nino*

Department of Materials Science and Engineering, University of Florida, Gainesville, FL 32611-6400, USA

Correspondence e-mail: jnino@mse.ufl.edu

The weberite structure ($A_2B_2X_7$) is an anion-deficient fluorite-related superstructure. Compared with fluorites, the reduction in the number of anions leads to a decrease in the coordination number of the B cations (VI coordination) with respect to the A cations (VIII coordination), thus allowing the accommodation of diverse cations. As a result, weberite compounds have a broad range of chemical and physical properties and great technological potential. This article summarizes the structural features of weberite and describes the structure in several different ways. This is the first time that the stacking vector and stacking angle are used to represent the weberite structure. This paper also discusses the crystallographic relationship between weberite, fluorite and pyrochlore (another fluorite-related structure). The cation sublattices of weberite and pyrochlore are correlated by an axial transformation. It has been shown that the different coordination environment of anions is due to the alternating layering of the AB_3 and A_3B close-packed cation layers. A stability field of weberite oxides is proposed in terms of the ratio of ionic radius of cations and relative bond ionicity. In addition, a selection of weberite compounds with interesting properties is discussed.

1. Introduction

The weberite crystal structure (space group: *Imma*, No. 74), with typical stoichiometry $A_2B_2X_7$ (A and B are cations, X is an anion, O or F), is a type of anion-deficient fluorite superstructure (AX_2). While several other compounds possess the same stoichiometry (pyrochlores, layered perovskites *etc.*), weberites are isomorphic with the mineral Na_2MgAlF_7. This mineral was originally found in Ivigtut in southwestern Greenland and was named after Theobald Weber (Bogvad, 1938). In 1944, Byström (1944) determined the crystal structure, basing his studies on the pyrochlore structure, which is another fluorite-related superstructure.

While the structure has a cationic sublattice arrangement similar to that found in the fluorite structure (face-centered cube), owing to distortions in the anion sublattice, the crystal structure has a high potential to accommodate diverse metals. The cations in (011) planes have nearly the same symmetry as in the hexagonal tungsten bronze (HTB) structure. In addition, the triangular network in $Na_2B^{2+}B^{3+}F_7$ weberites, which is formed by B^{2+} and B^{3+} cations in the HTB-like planes, potentially supports various magnetically ordered systems. To date, fluorine-based weberites such as $Na_2B^{2+}B^{3+}F_7$ and $Ag_2B^{2+}B^{3+}F_7$ have attracted most of the attention owing to their interesting magnetic properties (Cosier *et al.*, 1970; Dance *et al.*, 1974; Frenzen *et al.*, 1992; Laligant *et al.*, 1989; Laligant, Ferey *et al.*, 1987; Pankhurst *et al.*, 1991; Ruchaud *et

feature articles

Table 1
Weberite structure data (origin at A cations) in space group *Imma*.

Atoms	Wyckoff position	Site symmetry	Atomic position		
			x	y	z
$A1$	$4d$	$2/m$	0.25	0.25	0.75
$A2$	$4a$	$2/m$	0	0	0
$B1$	$4c$	$2/m$	0.25	0.25	0.25
$B2$	$4b$	$2/m$	0	0	0.5
$X1$	$8h$	m	0	y_1	z_1
$X2$	$16j$	1	x_2	y_2	z_2
$X3$	$4e$	$mm2$	0	0.25	z_3

$X1$ is at the center of A_3B, $X2$ is in the A_2B_2 tetrahedron and $X3$ is inside A_4B_2.

al., 1992; Thompson *et al.*, 1992; Tressaud *et al.*, 1974; Heger, 1973). Investigations on $A_2B_2O_7$ weberites have mainly focused on crystallography because of the close relationship between the weberite and the pyrochlore structures (Cordfunke & Ijdo, 1988; Groen & Ijdo, 1988; Klein *et al.*, 2006; Reading *et al.*, 2002; Astafev *et al.*, 1985; Bonazzi & Bindi, 2007; Desgardin *et al.*, 1976; Grey *et al.*, 2001, 2003; Grey & Roth, 2000; Ivanov & Zavodnik, 1990). Both of the structures form three-dimensional BX_6 networks and HTB-like layers. Some compounds, for example $Ca_2Sb_2O_7$, can form a metastable pyrochlore phase, which can be converted into the weberite structure by heating above 973 K (Brisse *et al.*, 1972). Recently, weberite oxides and weberite-related oxides have been reported to possess interesting physical properties (ferroelectric, dielectric and magnetic) as well as photocatalytic activity (Wakeshima *et al.*, 2004; Abe *et al.*, 2004, 2006; Cai & Nino, 2007; Cai *et al.*, 2007; Cava *et al.*, 1998; Ebbinghaus *et al.*, 2005; Ivanov *et al.*, 1998; Grey *et al.*, 2001; Lin *et al.*, 2006; Khalifah *et al.*, 1999; Nishimine *et al.*, 2004, 2005; Plaisier *et al.*, 2002; Wakeshima & Hinatsu, 2006; Hinatsu *et al.*, 2004; Harada & Hinatsu, 2002, 2001; Lam *et al.*, 2003; Wiss *et al.*, 2000; Wltschek *et al.*, 1996; Gemmill *et al.*, 2005).

There are a considerable number of publications on weberite ceramics. However, information on weberites is scattered. While presenting their work on the structure determination of $Na_2Fe_2F_7$, Yakubovich *et al.* (1993) devoted more than half of the paper to a comparison of different types of weberite structures in $Na_2B^{2+}B^{3+}F_7$ compounds and their relationship to the fluorite and the pyrochlore structures, but their discussion was limited to the crystallographic aspects. Lopatin *et al.* (1985) and Sych *et al.* (Sych, Kabanova, Garbuz *et al.*, 1988) focused on the stability-field region of these compounds. However, there is no article that correlates the structure and properties of weberites. Therefore, this paper is intended to provide a discussion of weberite ceramics, covering crystallographic aspects including the relationship between weberite, fluorite and pyrochlore, their stability field with respect to pyrochlore, and their interesting properties.

In §2 the structural features of weberite and the characteristics of weberite-like structures are discussed. Several different descriptions of the structure are given and a stacking vector and stacking angle are used for the first time to represent the weberite structure. The crystallographic relationship between the fluorite and the pyrochlore structures is

also discussed. It is also shown that the cation sublattices of pyrochlores can be transformed to the weberite-like lattice. The different stacking of neighboring AB_3 and A_3B layers lead to the different coordination environments of anions in weberite and pyrochlore. A stability field is developed to predict the formation of pyrochlore and weberite oxides. In §3 ferroelectric and dielectric properties of some weberite compounds are discussed.

2. Crystal structure

2.1. Classic orthorhombic weberite

The space group of the orthorhombic weberite structure is *Imma* (No.74) with four formula units per unit cell ($Z = 4$). However, the correct space group of weberites was a subject of controversy for a long time, as it was described as both *Imma* and *Imm*2 (Sych, Kabanova & Andreeva, 1988; Haegele *et al.*, 1978; Giuseppetti & Tadini, 1978; Knop *et al.*, 1982; Byström, 1944). The detailed history of the determination of the space group has been reported by Yakubovich *et al.* (1993). The two space groups are closely related as *Imm*2 is a subgroup of *Imma*. The only evidence ruling out *Imma* was the observation of very weak ($hk0$) with $h = 2n + 1$ reflections. It was later proven that the existence of ($hk0$) with $h = 2n + 1$ reflections from Na_2NiFeF_7 single crystals and Na_2NiAlF_7 originated from the Renninger effect ('double reflection' process; Schmidt *et al.*, 1992; Laligant *et al.*, 1989). Thus, there is no doubt that the true space group of the orthorhombic weberite is *Imma*. The atomic positions and site symmetry are given in Table 1.

In weberites the A ions sit in the $4a$ and $4d$ atomic positions with site symmetry $2/m$ and establish a coordination number of 8 with the anions. The A ions have two different coordination environments. The $A1$ cations (in atomic position $4d$) lie in a highly distorted cube (or square prism) where there are two different $A1-X$ bond lengths. The cubes are edge-shared to form a series of chains in the [100] direction. The $A2$ cations (in atomic position $4a$) are located within bi-hexagonal pyramids in which anions are spaced at three different distances from the central cations. Each pyramid is corner-shared with two other pyramids and edge-shared with four $A1X_8$ cubes. As presented in Table 1 there are three Wyckoff positions for anions ($X1$ at $8h$, $X2$ at $16j$ and $X3$ at $4e$). $A1$ ions only connect to $X1$ and $X2$, while $A2$ link to all three types of anions (two $X1$, four $X2$ and two $X3$).

The B ions are located in the $4b$ and $4c$ Wyckoff positions (site symmetry $2/m$) and have a coordination number of 6, *i.e.* $A_2^{VIII}B_2^{VII}X_7$. The weberite structure can be described as a network of corner-shared BX_6 octahedra with the penetration of A cations (see Fig. 1). There are two types of BX_6 octahedra: B-1 (B^{2+} in the case of $A_2B^{2+}B^{3+}F_7$, A = Na$^+$ or Ag$^+$) in $4c$ Wyckoff positions, and B-2 (B^{3+} in the case of $A_2B^{2+}B^{3+}F_7$) in $4b$ Wyckoff positions. Each of the six vertices of B-1 octahedra connects to another B octahedron, while only four vertices of a B-2 octahedron link to other B octahedra. The two unpaired vertices are in a *trans* configuration. As will be

discussed later, trigonal or monoclinic weberite variants cause a *cis* configuration (see Fig. 2). The *B*-1 octahedra are corner-linked to each other and form *B*-1 octahedral chains parallel to the *A*1 chains (in the [100] direction). The *B*-2 octahedra are isolated from each other and link the *B*-1 octahedral chains to form a three-dimensional octahedral network.

The arrangements of *A* and *B* ions lead to three different cation tetrahedra. Six anions occupy the two A_3B (A_3BX, $X1$) and four A_2B_2 tetrahedral interstices (A_2B_2X, $X2$) and none are located inside the two AB_3 sites ($AB_3[]$, where [] represents a vacant site) in a formula unit. The remaining anion ($X3$) maintains four coordination and lies outside the two edge-shared AB_3 tetrahedra, very close to the shared B–B

edge (see Fig. 3). $X3$ can also be considered to sit inside the octahedron (A_4B_2), which shares faces with two adjacent AB_3 tetrahedra, and distort towards the B–B edge (Grey *et al.*, 2003).

The weberite structure can also be considered as a stacking of repeated layers or slabs. The most common way to examine the structure is to view it as stacked, alternating close-packed metal layers A_3B and AB_3 on (011) parallel planes. In A_3B layers, four *A*-1 and two *A*-2 ions form a hexagonal ring with *B*-2 occupying the center. In other words the *A* cations form Kagomé-type networks. [Kagomé in Japanese means a bamboo-basket woven pattern. It is formed by interlaced triangles and each lattice point has four equivalent bonds. 'Kagomé' was introduced by Husimi after he and his co-
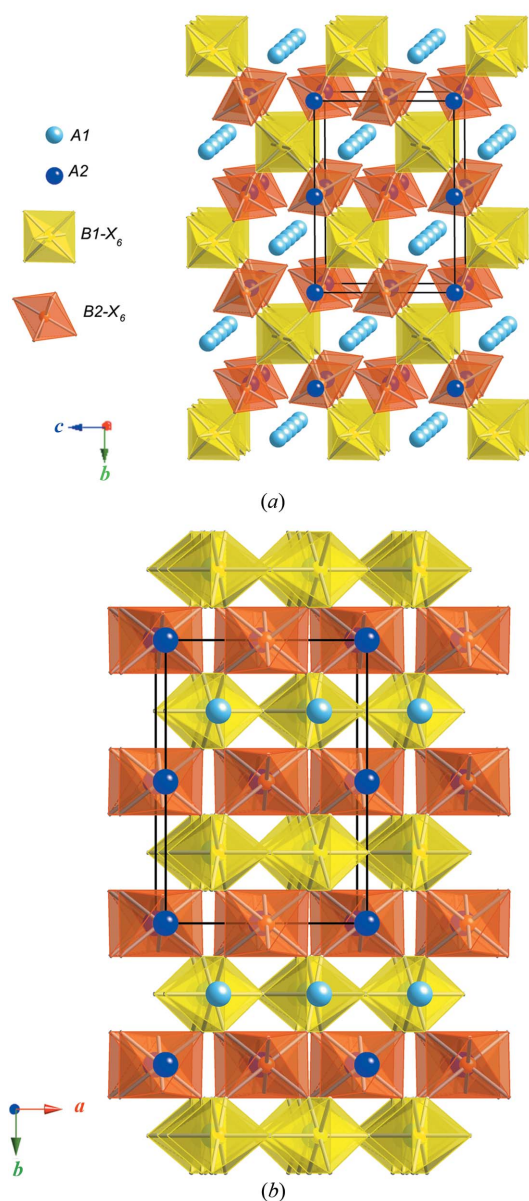

(a)

(b)

Figure 1
B-octahedral network and *A* cations (*a*) in the [1, 0.04, 0.07] direction and (*b*) in the [0.1, 0, 1] direction; the black lines are the unit cell.
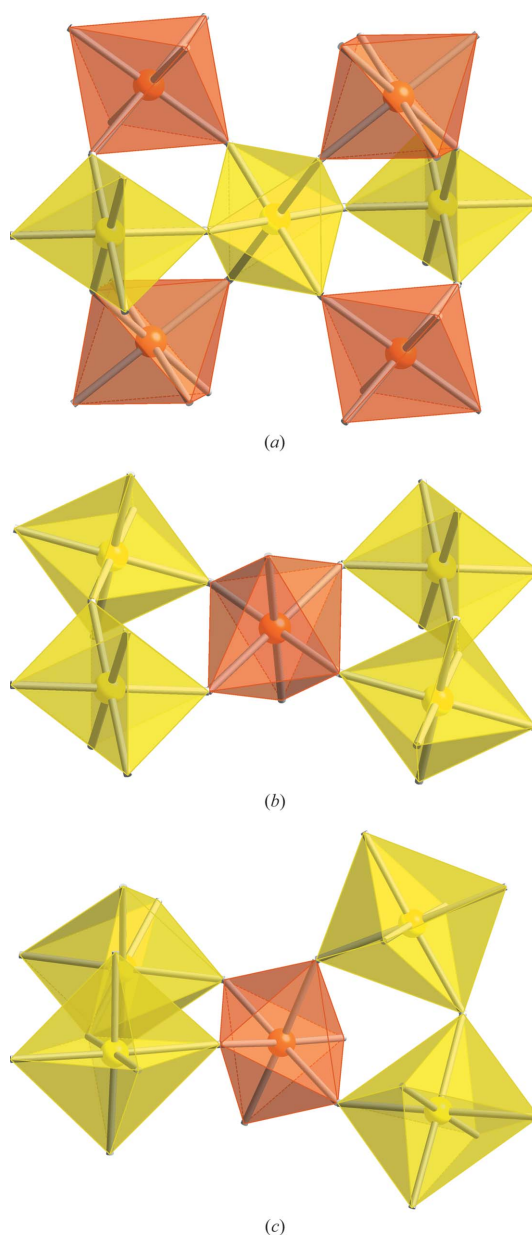

(a)

(b)

(c)

Figure 2
(*a*) A *B*-1 octahedron in the center and its connection to another six octahedra; (*b*) *trans* configuration of *B*-2 octahedra; (*c*) *cis* configuration of *B*-2 octahedra.

feature articles

worker Syôzi found a new antiferromagnetic lattice by star-to-triangle transformation from a honeycomb lattice (Mekata, 2003). Syôzi published the first Kagomé paper in 1951 (Syozi, 1951); see Fig. 4.] In AB_3 layers the BX_6 octahedron arrangement is nearly identical with the basal plane of the hexagonal tungsten bronze (HTB) structures and A-2 cations are in the center of the hexagonal rings. The HTB-like layers can also be simplified by a Kagomé net representation (Fig. 5). The HTB-like layers are displaced with respect to each other by an interlayer stacking vector (SV) which is defined as the projected distance, viewed down the (pseudo-) sixfold axis, between crystallographically similar ions in adjacent layers. White (1984) and Cohelho et al. (1997) used SV as an alternative description for zirconolite, zirkelite, pyrochlore and polymignyte. Here, SV is used to describe weberite. The

stacking vectors in the weberite structure are nearly in the $[0\bar{1}1]$, $[\bar{3}1\bar{1}]$ and $[31\bar{1}]$ directions. They are typically of the order 4 Å. The angle between successive stacking vectors (SA) is approximately 120°. The distance between two neighboring HTB-like layers along the (pseudo-) sixfold axis is approximately 5.8 Å. Fig. 6 shows the stacking vectors between three sequences of HTB layers.

There is yet another way to consider the weberite repeated layers. The first layer is formed by the alternating B-1 octahedral chains and A-1 distorted cube (or square prism) chains, which are in the [100] direction for classic orthorhombic weberites. In this layer the B-1 octahedra are edge-shared with
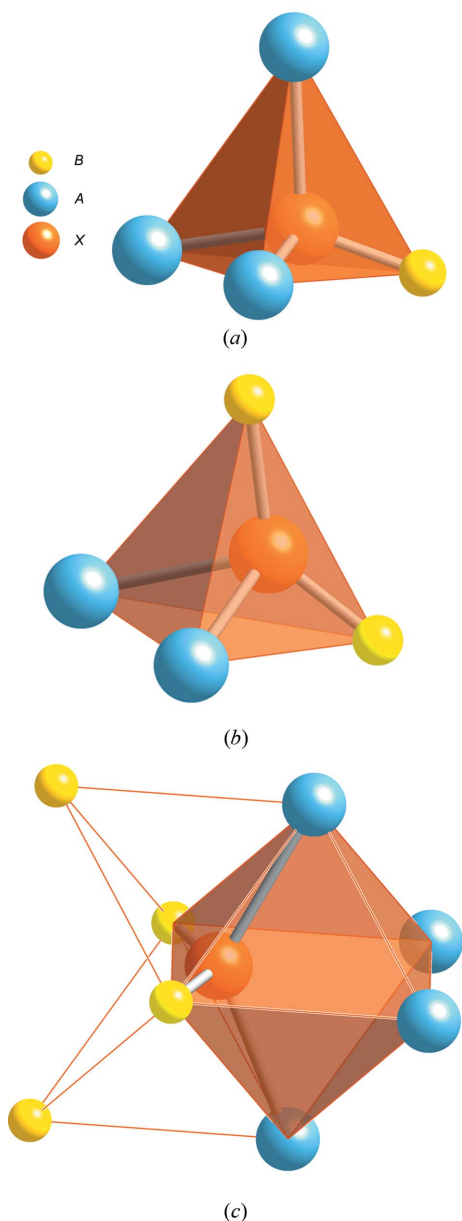

Figure 3
Anion coordination: (a) X-1 in A_3B; (b) X-2 in A_2B_2; (c) X-3 in A_4B_2.
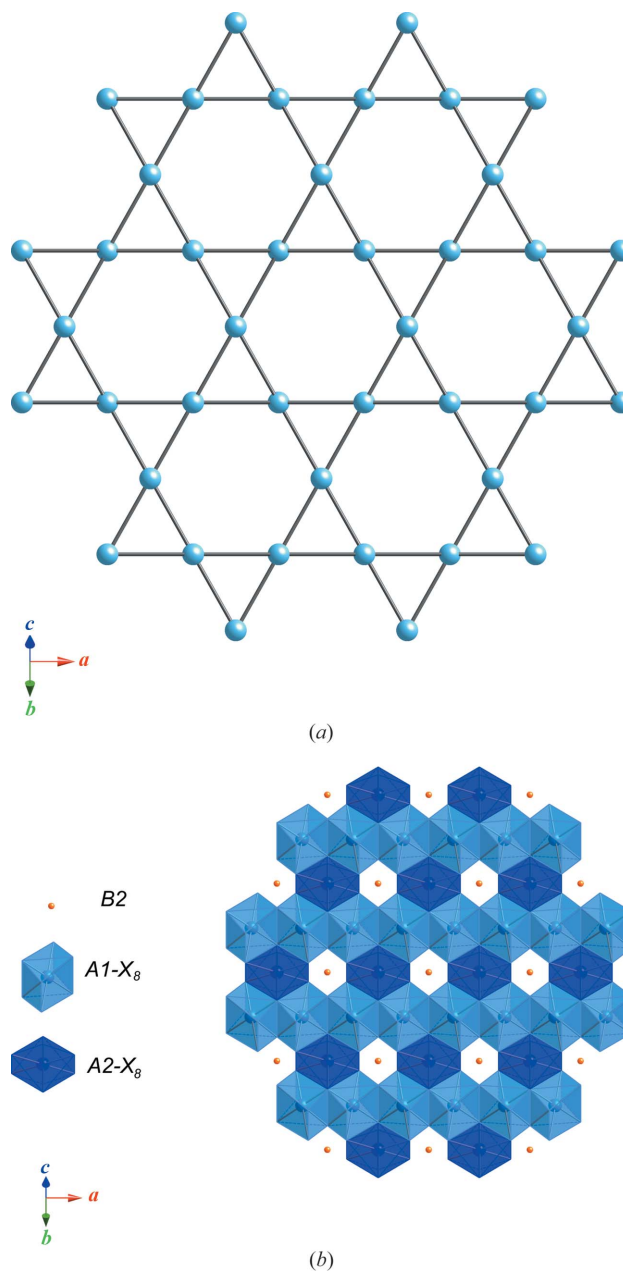

Figure 4
(a) Kagomé net presentation of A cations on A_3B layers; (b) AX_8 polyhedral representation of A_3B layers, which are parallel to the (011) plane.

A-1 cubes. The second layer is alternating *B*-2 octahedra and *A*-2 bi-hexagonal pyramids in the [100] direction as in Fig. 7 (Rossell, 1979; Renaudin *et al.*, 1988).

2.2. Relationship to fluorite and pyrochlore

Weberite and pyrochlore ($A_2B_2X_7$) are both fluorite-related (AX_2 or A_4X_8) superstructures. The coordination number of *A* and *B* is the same in both structures. These two structures have a similar cationic sublattice, which is comprised of stacked cubic close-packed cation layers, the same as (111) planes in fluorite. These layers alternate between the compositions A_3B and AB_3 and are parallel to (111) planes in pyrochlore and

(011) planes in weberite. AB_3 layers in pyrochlore can also be described as HTB-like layers. The length of SV and the value of SA of the pyrochlore structure are almost the same as weberite. However, the difference between the weberite and the pyrochlore structures is the different stacking of two successive AB_3 and A_3B layers, which will be discussed later in this section. The crystallographic relationship between the weberite and the pyrochlore structures is further confirmed by the fact that the space group of weberite (*Imma*) is a subgroup of $Fd\bar{3}m$, the space group of pyrochlore. If the lattice parameter of pyrochlores is $2a$ with respect to fluorite a ($a \simeq 5$ Å), then the lattice parameters of the classic orthorhombic

Figure 6
Left: Stacking vectors (black arrows) between three sequences of HTB layers; right: Kagomé nets of three successive HTB layers (purple arrows are stacking vectors). This figure is in color in the online version of this paper.
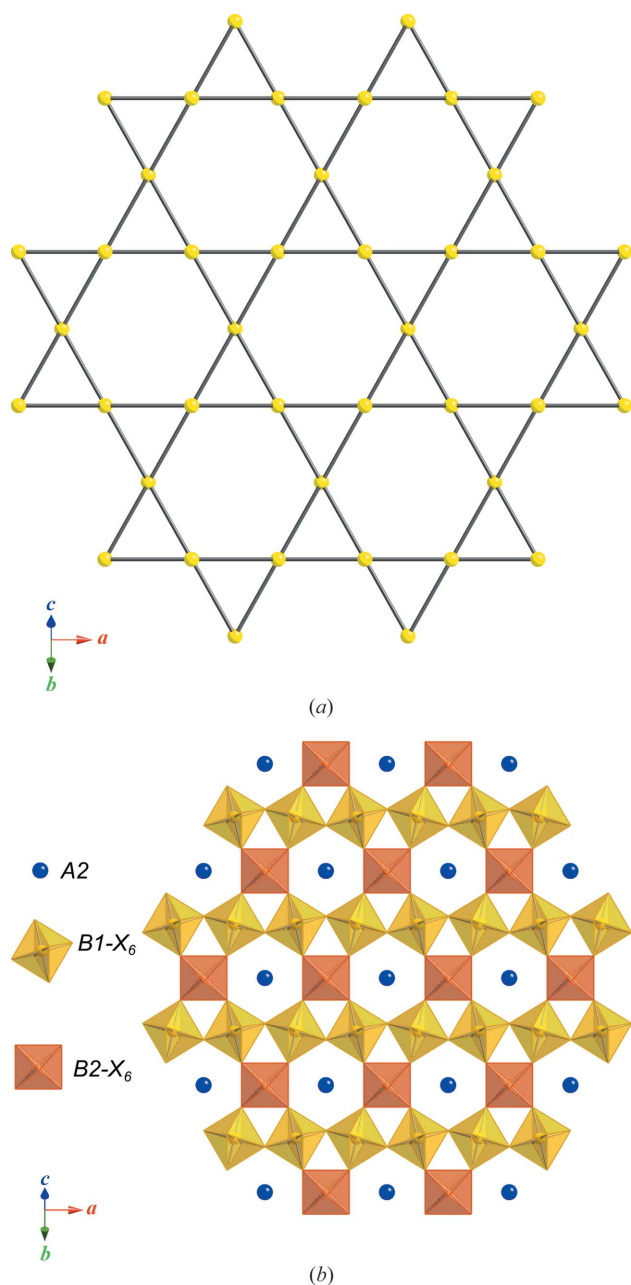

Figure 5
(*a*) Kagomé net presentation of *B* cations on AB_3 layers; (*b*) BX_6 polyhedral representation of AB_3 layers, which are parallel to the (011) plane.
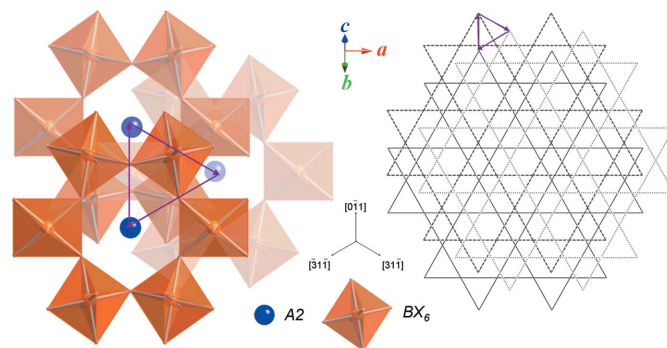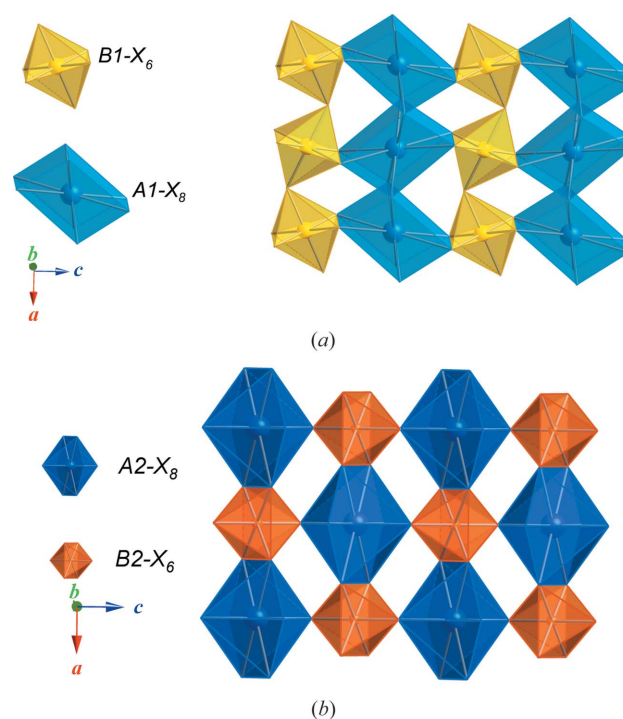

Figure 7
(*a*) The layer consisting of *A*1 and *B*1 lines; (*b*) *A*-2 and *B*-2 layers, viewed in the [010] direction.

　　Lu Cai and Juan C. Nino · Complex Ceramic Structures. I　　**273**

Table 2
Pyrochlore ($A_2B_2X_6X'$) structure data in space group *Imcm*.

Atoms	Wyckoff position	Site symmetry	Atomic position		
			x	y	z
A	4b	2/m	0	0.5	0
	4c	2/m	0.25	0.25	0.25
B	4a	2/m	0	0	0
	4d	2/m	0.25	0.75	0.25
X	4e	mm2	0.5	$x + 0.25$	0.25
	4e	mm2	0	x	0.25
	16j	1	$x - 0.125$	0.125	$x + 0.125$
X'	4e	mm2	0.25	0.375	0

The x is the oxygen parameter inside the A_2B_2 tetrahedral site. The value is between 0.3125 and 0.375.

(a)

(b)

(c)

(d)

Figure 8
(*a*) Cationic network on (111) of fluorite; (*b*) AB_3 layer; (*c*) A_3B layer on (011) of weberite; dashed lines are the unit cell; (*d*) axial transformation of pyrochlore to weberite [black dashed lines: a fluorite cell; blue lines: double pyrochlore cells; red dotted lines: weberite lattice; green shadow $(011)_w$ and $(111)_p$]. This figure is in color in the online version of this paper.

weberites are approximately $2^{1/2}a$, $2a$ and $2^{1/2}a$. The rotation of $45°$ about the b axis of the pyrochlore cation sublattice leads to the weberite-like cation sublattice (Fig. 8). The (111) planes of pyrochlore are transformed to the (011) of the new lattice. The transformation relationship can be written as

$$W = P \begin{pmatrix} 0.5 & 0 & 0.5 \\ 0 & 1 & 0 \\ -0.5 & 0 & 0.5 \end{pmatrix}. \quad (1)$$

The transformation leads to the space group *Imcm*, which is a different setting of *Imma*. The *Imma* lattice can be achieved by the $90°$ rotation of the coordinate system of *Imcm*. The transformation matrix is

$$\begin{pmatrix} 0 & 1 & 0 \\ 0 & 0 & 1 \\ 1 & 0 & 0 \end{pmatrix}. \quad (2)$$

The resulting lattice parameters in *Imma* are $2a$, $2^{1/2}a$ and $2^{1/2}a$. In order to match the weberite lattice parameters, the space group *Imcm* is preferred when presenting the atomic positions of pyrochlore in the weberite-like orthorhombic lattice (Table 2).

It is easy to recognize weberite and distinguish the three structures from powder diffraction. As is well known, in Cu $K\alpha$ radiation to $2\theta \simeq 70°$, the five fluorite characteristic peaks are (111), (200), (220), (311) and (222). The (111) reflection is at $2\theta \simeq 30°$ with the highest intensity. In pyrochlore, owing to the doubling of the lattice parameter with respect to fluorite, the five fluorite peaks become (222), (400), (440), (622) and (444). The appearance of several weak reflections, especially the (111) peak at $2\theta \simeq 15°$, is a major difference between the X-ray diffraction (XRD) patterns of fluorite and pyrochlore. In orthorhombic weberite, the five fluorite peaks are split, for example, the most intense $(111)_f$ or $(222)_p$ are split into $(022)_w$ and $(220)_w$. There are several more reflections in weberite, which are systematic absences in pyrochlore, for example, $(101)_w$ and $(020)_w$ [corresponding to $(200)_p$]. Details on the XRD reflection for fluorite, pyrochlore and
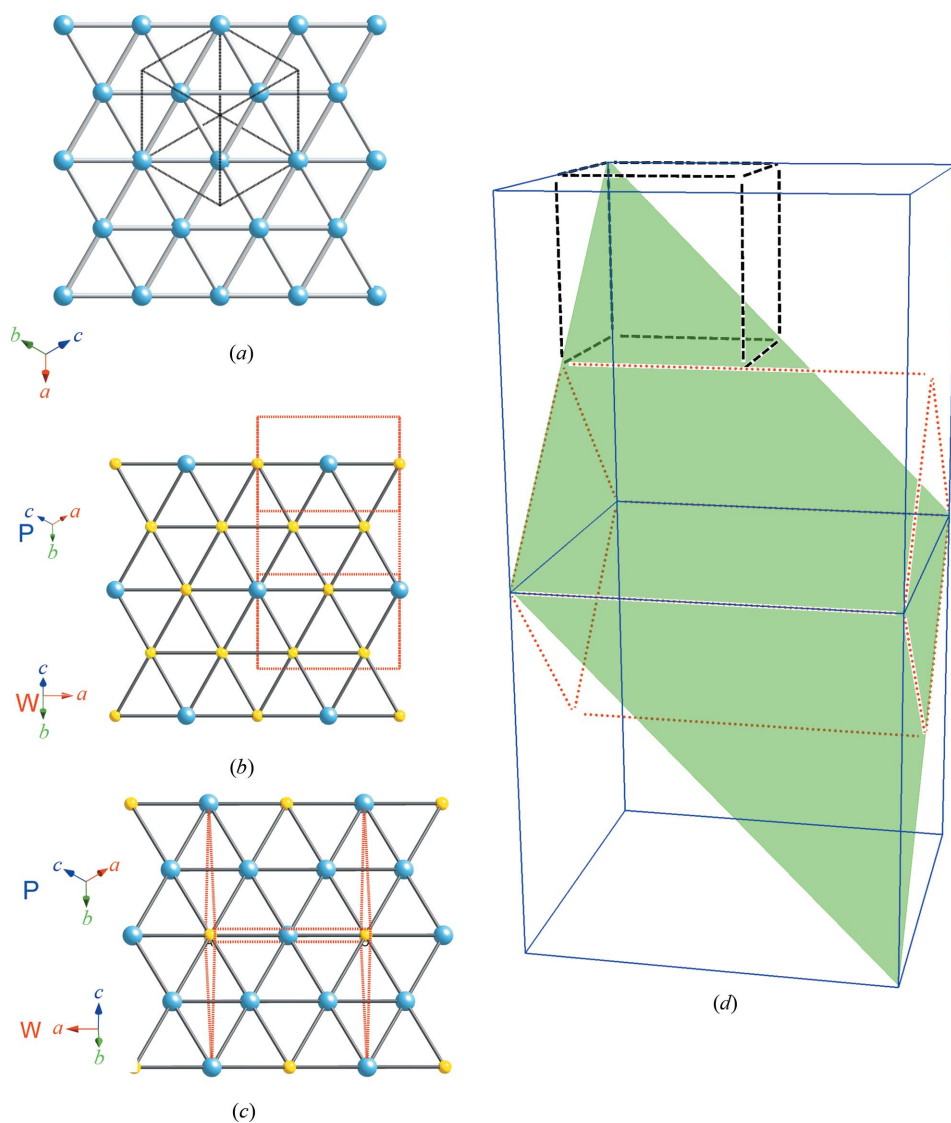
weberite are listed in Table 3. For space reasons, only reflections up to $(222)_f$ are presented.

It is important to recall that in fluorites, each anion is at the center of the cationic tetrahedra (A_4X). The arrangement of A and B leads to different cation tetrahedra: AB_3, A_3B and A_2B_2 in weberites, and A_4, B_4 and A_2B_2 in pyrochlores. The reason for the formation of different cation tetrahedra is that weberites and pyrochlores are different in stacking two neighboring AB_3 and A_3B layers, although generally they follow the pattern of cubic close-packed cation layers. The three nearest-neighbor metal ions in these layers form pseudo-equilateral triangles. The distribution of A and B cations in AB_3 layers will lead to two types of triangles: AB_2 and B_3. The cations in the following A_3B layer lie above the centers of these triangles. If an AB_3 layer is a reference, there are $2^{1/2}a/2$ along $[100]_w$ or $[10\bar{1}]_P$ displacement in the above A_3B layer between weberite and pyrochlore. As a result, in the A_3B layer, A cations are above the center of AB_2 triangles and B cations are above B_3 triangles in pyrochlore, while in weberite, 2/3 A (A-1) and all B cations are above the AB_2 triangles and the remaining A cations (A-2) are above B_3 triangles (see Fig. 9). Therefore, these arrangements lead to two AB_3, two A_3B and four A_2B_2 in a formula unit of weberite, and in the case of pyrochlore, one A_4, six A_2B_2 and one B_4. In addition, different stacking of two neighboring AB_3 and A_3B layers can explain why the transformation of the pyrochlore cation sublattice into a weberite-like lattice results in a different setting of the space group.

As stated in §2.1, in a formula unit the $X3$ anion of weberite is located outside the cation tetrahedra and leaves two AB_3 tetrahedra with a vacant center. In contrast, all anions in the pyrochlore structure are inside the cation tetrahedra. Therefore, it can be argued that pyrochlore is more closely related to fluorite than weberite since the former preserves all the anions in cation tetrahedral interstices (Yakubovich *et al.*, 1993; Grey *et al.*, 2003). In weberite it is understandable that the X-deficient site is more favorable in B-rich tetrahedra (AB_3 than A_2B_2 and A_3B), because B ions have a smaller coordination number (CN). However, it raises the question: why there are two AB_3 tetrahedra with a vacant center and the $X3$ is not inside the cation tetrahedra? Grey *et al.* (2003) argued that in $Ca_2Ta_2O_7$ weberite, the sum of valence ($\sum v/CN$) in $CaTa_3$ tetrahedra is so highly over-saturated that $CaTa_3$ cannot accommodate $X3$. Actually, the highly over-saturated AB_3 tetrahedra occur in all weberite compounds: $A_2^{1+}B^{2+}B^{3+}F_7$, $A_2^{2+}B_2^{5+}O_7$ and $A_2^{1+}B_2^{6+}O_7$. The nominal sum of valence in the center of AB_3 is 1.46 for $A_2^{1+}B^{2+}B^{3+}F_7$, 2.75 for $A_2^{2+}B_2^{5+}O_7$, 3.13 for $A_2^{1+}B_2^{6+}O_7$. Thus, anions should distort largely towards A cations to meet the required valence, which would then result in a shorter $A-X$ distance than a $B-X$ distance. However, A ions are larger and have a larger CN than B ions and so the $A-X$ bond length should be larger than the $B-X$ bond length. The end result is that anions cannot move towards A cations and the required valence cannot be achieved. By contrast, the sum of valence in the center of AB_3 is under-saturated, being 0.875 for $A_2^{1+}B^{2+}B^{3+}F_7$, 1.58 for $A_2^{2+}B_2^{5+}O_7$ and 1.375 for $A_2^{1+}B_2^{6+}O_7$. Anions are required to

move towards B cations, which is favored by the bond length argument above. As for A_2B_2 tetrahedra, the sum of valence is 1.08 for $A_2^{1+}B^{2+}B^{3+}F_7$, 2.17 for $A_2^{2+}B_2^{5+}O_7$ and 2.25 for $A_2^{1+}B_2^{6+}O_7$. In this case the sum of valence is close to the anion oxidation state.

In order to check the stability of the $X3$, the empirical equation by Brese & O'Keeffe (1991) is used to calculate the valence of the $X3$

Table 3
XRD reflections for fluorite, pyrochlore and weberite.

hkl (fluorite)	hkl (pyrochlore)	hkl (weberite)	Corresponding pyrochlore plane
	111	011	111
		101	200
		020	020
	220	002	202
		121	220
		200	$20\bar{2}$
	311	112	$31\bar{1}$
		211	311
		031	131
111	222	022	222
		220	$22\bar{2}$
200	400	202	400
		040	040
	331	013	313
		132	331
		231	$33\bar{1}$
		103	402
		222	420
		301	$40\bar{2}$
		141	240
		123	422
		042	242
		321	$42\bar{2}$
		240	$24\bar{2}$
	333	033	333
	511	213	511
		312	$51\bar{1}$
		051	151
220	440	004	404
		242	440
		400	$40\bar{4}$
	531	114	513
		233	531
		152	351
		332	$53\bar{1}$
		251	$35\bar{1}$
		411	$51\bar{3}$
	442	024	424
		143	442
		341	$44\bar{2}$
		420	$42\bar{4}$
		303	600
		060	060
	620	204	602
		323	620
		402	$60\bar{2}$
		161	260
	533	134	533
		053	353
		431	$53\bar{3}$
311	622	224	622
		062	262
		422	$62\bar{2}$
		260	$26\bar{2}$
222	444	044	444
		440	$44\bar{4}$

$$V_i = \sum v_{ij} = \sum \exp((R_{ij} - r_{ij})/b) \qquad (3),$$

where R_{ij} is the bond-valence parameter, r_{ij} is the bond distance and b is a constant. Three representative compounds were chosen for detailed analysis: $Na_2^{1+}Mg^{2+}Al^{3+}F_7$, $Sr_2^{2+}Sb_2^{5+}O_7$ and $Ag_2^{1+}Te_2^{6+}O_7$. There are few, if any, reported bond-length data for $Ag_2B_2F_7$. Na_2MgAlF_7 was chosen since it is the aristotype of the weberite compounds. The r_{ij} of $Na_2^{1+}Mg^{2+}Al^{3+}F_7$ is from Knop *et al.* (1982) based on single-crystal XRD. $Sr_2^{2+}Sb_2^{5+}O_7$ was chosen because it is a stable weberite even under high pressure and neutron diffraction data are available (Knop *et al.*, 1980; Groen & Ijdo, 1988). As for $A_2^{1+}B_2^{6+}O_7$ compounds, only the crystal structure $Ag_2Te_2O_7$ has been reported (Klein *et al.*, 2006). Table 4 lists the detailed valence information including all three anion types as well as cations by the empirical equation above using the bond-valence parameters (Brese & O'Keeffe, 1991; Brown, 2002) and the bond lengths (r_{ij}) from the literature. The valence of

$X3$ is close to its oxidation state in these compounds. It is worth noting that the discrepancy is small in $Ag_2^{1+}Te_2^{6+}O_7$ for all three oxygen anions. Therefore, $A_2^{1+}B_2^{6+}O_7$ weberites are possible.

Another significant difference is the formation of BX_6 networks. All of the anions in weberites participate in the formation of BX_6 octahedra, but only 6/7 of the anions in pyrochlores do. The BX_6 octahedral network in both structures is fairly rigid. Therefore, in order to maintain the octahedral network it is difficult for the weberite to form vacancies at anion sites. By contrast, the pyrochlore structure tolerates X deficiency or paired A and X deficiencies relatively easily. Examples of such pyrochlore oxides are $Bi_{1.5}Zn_{0.92}Nb_{1.5}O_{6.92}$ and $Tl_2B_2O_6$ (B = Nb, Ta and U), $Tl_2Os_2O_{7-x}$ and $Pb_2Os_2O_{7-x}$ (Nino, 2002; Subramanian *et al.*, 1983; Reading *et al.*, 2002). In addition, the substitution of small amounts of oxygen by F^- may prevent the formation of weberites. For example, $Ca_2Sb_2O_7$ pyrochlore transforms into weberite irreversibly
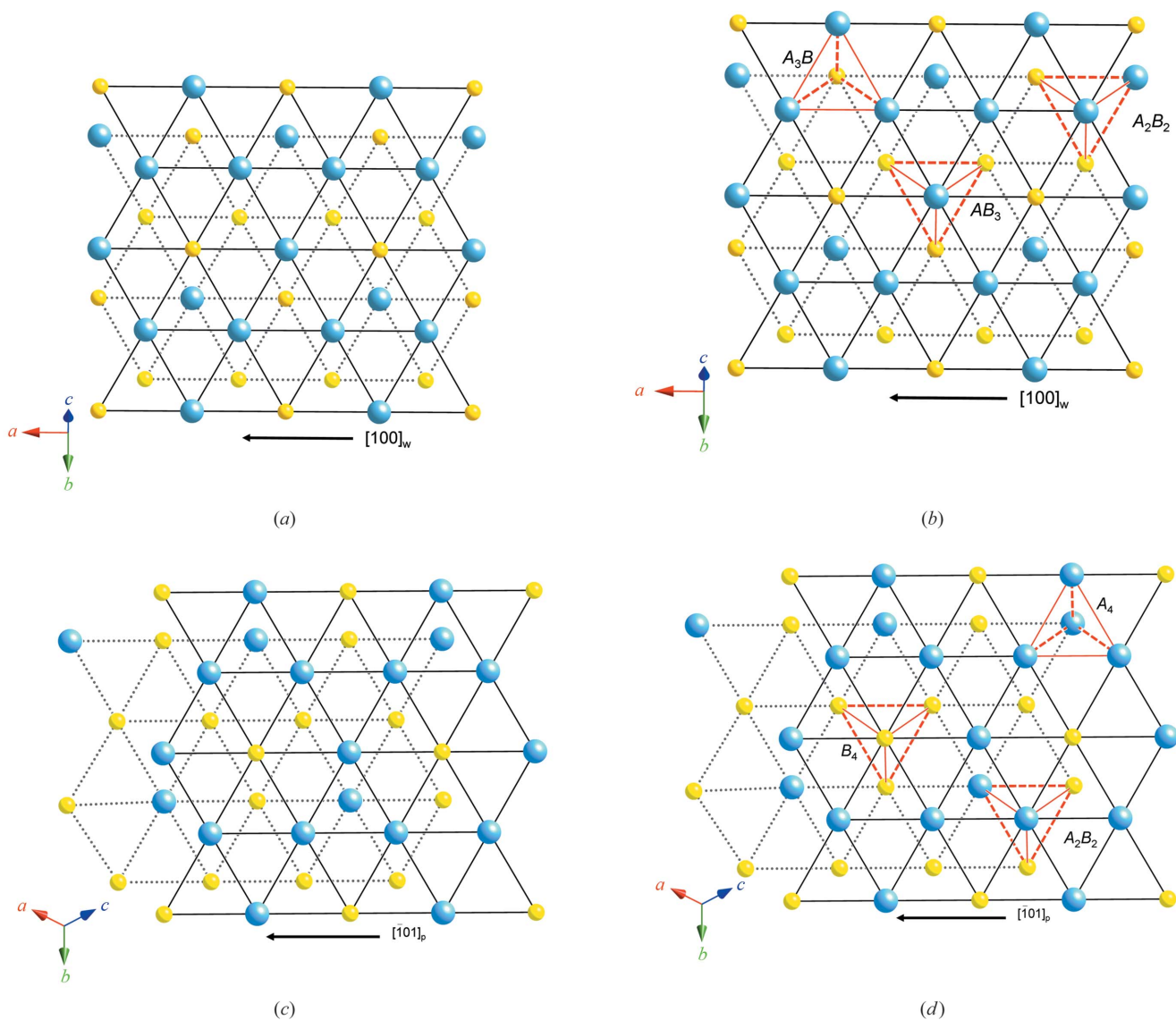

Figure 9
A_3B and AB_3 slabs of (*a*) weberite and (*b*) pyrochlore. Cations connected by dotted lines are on the AB_3 layer and by grey lines are on the A_3B layer. The red lines (or dotted line) show cation tetrahedra. This figure is in color in the online version of this paper.

Table 4
Examples of bond-valence sum for anions and cations by Brese and O'Keeffe.

$X1$ in A_3B tetrahedra				$X2$ in A_2B_2 tetrahedra				$X3$ outside the AB_3 tetrahedra			
Bonds	r_{ij} (Å)	v_{ij}	$\sum v_{ij}$	Bonds	r_{ij} (Å)	v_{ij}	$\sum v_{ij}$	Bonds	r_{ij} (Å)	v_{ij}	$\sum v_{ij}$
Na_2MgAlF_7											
Al—F	1.825	0.469		Mg—F	1.960	0.360		Mg—F	1.951	0.368	
Na2—F	2.211	0.236		Al—F	1.793	0.512		Mg—F	1.951	0.368	
Na1—F	2.423	0.133	0.972	Na2—F	2.549	0.095	1.022	Na2—F	2.689	0.065	0.866
Na1—F	2.423	0.133		Na1—F	2.749	0.055		Na2—F	2.689	0.065	
$Na1^{1+}$: $\sum v_{ij}$ = 0.779; $Na2^{1+}$: $\sum v_{ij}$ = 0.981; Mg^{2+}: $\sum v_{ij}$ = 2.17; Al^{3+}: $\sum v_{ij}$ = 2.89											
$Sr_2Sb_2O_7$											
Sb2—O	1.922	1.056		Sb1—O	1.971	0.926		Sb1—F	2.005	0.843	
Sr2—O	2.363	0.515		Sb2—O	2.202	0.512		Sb1—F	2.005	0.843	
Sr1—O	2.502	0.354	2.280	Sr1—O	2.833	0.145	2.151	Sr2—F	2.850	0.138	1.963
Sr1—O	2.502	0.354		Sr2—O	2.599	0.273		Sr2—F	2.850	0.138	
$Sr1^{2+}$: $\sum v_{ij}$ = 1.996; $Sr2^{2+}$: $\sum v_{ij}$ = 2.40; $Sb1^{5+}$:$\sum v_{ij}$ = 5.39; $Sb2^{5+}$: $\sum v_{ij}$ = 5.34											
$Ag_2Te_2O_7$											
Te2—O	1.825	1.281		Ag1—O	2.806	0.067		Ag2—O	2.806	0.067	
Ag2—O	2.388	0.207		Ag2—O	2.549	0.134		Ag2—O	2.806	0.067	
Ag1—O	2.465	0.168	1.864	Te1—O	1.997	0.806	2.041	Te1—O	1.946	0.925	1.983
Ag1—O	2.465	0.168		Te2—O	1.905	1.034		Te1—O	1.946	0.925	
$Ag1^{1+}$: $\sum v_{ij}$ = 0.939; $Ag2^{1+}$: $\sum v_{ij}$ = 1.084; $Te1^{6+}$: $\sum v_{ij}$ = 5.785; $Te2^{6+}$: $\sum v_{ij}$ = 5.983											

r_{ij} is the bond distance, v_{ij} is the bond valence.

above 973 K, but $CaNaSb_2O_6F$ and $Ca_{1.56}Sb_2O_{6.37}F_{0.44}$ pyrochlores are stable (Aleshin & Roy, 1962; Aia *et al.*, 1963).

2.3. Weberite-like structures

The weberite structures show a wide variety of different modifications including monoclinic and trigonal variants. Grey *et al.* (2003) proposed the use of the nomenclature of the International Mineralogical Association Commission New Minerals and Mineral Names (IMA-CNMMN), which was initially approved for zirconolite $CaZrTi_2O_7$ (Bayliss *et al.*, 1989). As discussed above, the basic building unit is a slab formed by one A_3B and one AB_3 layer. The differences between weberites are the crystal system and the number of slabs (N) in a unit cell. A notation which combines N and the first letter of the crystal system is used to indicate different weberites. For example, the notation of the classic orthorhombic weberite is $2O$ because it has two slabs in a unit cell. The reported weberites include $2O$, $2M$, $3T$, $4M$, $5M$, $6M$, $6T$, $7M$ and $8O$. Tables 5 and 6 list different types of $A_2B_2F_7$ and $A_2B_2O_7$ weberites, respectively. $(NaCu)Cu_2F_7$ (or $NaCu_3F_7$, space group $C2/c$) and $(Ca_{0.5}Ln_{1.5})(Ca_{0.5}Sb_{1.5})O_7$ (or $CaLn_{1.5}Sb_{1.5}O_7$, space group $I2/m11$, Ln = La, Pr, Nd and Y) are special $2M$ weberites and more like pseudo-$2O$ weberites for they maintain the structural feature of $2O$ rather than $2M$, as will be discussed later. $Ca_2Ta_2O_7$-based compounds are important in the weberite family since for $N > 4$, only $Ca_2Ta_2O_7$-based compounds have been reported. Grey and co-workers (Grey *et al.*, 1999, 2001, 2003; Grey & Roth, 2000) have shown that $Ca_2Ta_2O_7$ compounds can crystallize into $3T$, $4M$, $5M$, $6T$, $6M$ and $7M$ by different doping or synthesis methods and later Ebbinghaus *et al.* (2005) also synthesized an

$8O$ $Ca_2Ta_2O_7$ single crystal using the optical floating zone method.

A significant difference between $2O$ and non-$2O$ weberites is that the AB_3 and A_3B layers are parallel to the (011) planes for $2O$ and parallel to the (001) planes for other weberites, except for $NaCu_3F_7$ and $CaLn_{1.5}Sb_{1.5}O_7$ (Ln = La, Pr, Nd and Y). The formula unit (Z) of $NaCu_3F_7$ and $CaLn_{1.5}Sb_{1.5}O_7$ is also consistent with $2O$ weberites, four rather than eight, the latter the formula unit for other $2M$ weberites. As in §2.2 the lattice parameters of $2O$ weberites are approximately $2^{1/2}a$, $2a$ and $2^{1/2}a$ ($a \simeq 5$ Å, the lattice parameters for fluorite). The lattice parameters of $2M$ weberites are nearly $6^{1/2}a$, $2^{1/2}a$ and $6^{1/2}a$. The $[0\bar{1}1]$, [100] and [011] vectors of $2O$ become [100], [010] and [001] of $2M$. The lattice parameter difference between $2M$, $4M$, $5M$, $6M$ and $7M$ is mainly on the c axis. The lattice parameters for nM (n = 2, 4, 5 and 7) are approximately $6^{1/2}a$, $2^{1/2}a$ and $[n(6)^{1/2}/2]a$ and they are nearly $2^{1/2}a$, $6^{1/2}a$ and $3(6)^{1/2}/a$ for $6M$ (Grey *et al.*, 1999, 2001, 2003; Grey & Roth, 2000). The $8O$ weberite is closely related to a monoclinic variant rather than $2O$ in both the orientation of the AB_3 and A_3B layers and the lattice parameters. The lattice parameters are nearly $2^{1/2}a$, $6^{1/2}a$ and $4(6)^{1/2}/a$. As for $3T$, the [100], [−0.5,−0.5, 0.5] and [012] vectors in $2O$ are transformed into the basal vectors. The resulting lattice parameters are approximately $2^{1/2}a$, $2^{1/2}a$ and $2(3)^{1/2}a$. The relationship of $2O$, $2M$ and $3T$ weberites is shown in Fig. 10. Meanwhile, the lattice parameters of $6T$ are approximately $2^{1/2}a$, $2^{1/2}a$ and $4(3)^{1/2}a$, just double the length of the basal vector in the c axis.

For $2O$ weberites there are two special types in which the body-center symmetry is lost. The first case is when Cu^{2+} is introduced into $Na_2B^{2+}B^{3+}F_7$ at B-1 sites such as Na_2CuCrF_7 and Na_2CuInF_7 (Kummer *et al.*, 1988; Ruchaud *et al.*, 1992). The common Jahn–Teller distortion (the CuF_6 octahedra are

Table 5
List of $A_2B_2F_7$ weberites.

Type		Space group	Z	a (Å)	b (Å)	c (Å)	β (°)	R_A (Å)	R_B (Å)	R_A/R_B	Properties investigated
2O	Na₂MgCrF₇ (Chassain, 1969)	Imma	4	7.39	7.15	10.20		1.18	0.667	1.768	
2O	Na₂MgGaF₇ (Chassain, 1969)	Imma	4	7.42	7.16	10.16		1.18	0.67	1.761	
2O	Na₂MgScF₇ (Chassain, 1969)	Imma	4	7.55	7.34	10.43		1.18	0.733	1.611	
2O	Na₂MgVF₇ (Chassain, 1969)	Imma	4	7.45	7.24	10.30		1.18	0.68	1.735	
2O	Na₂NiFeF₇ (Cosier et al., 1970; Laligant et al., 1989; Thompson et al., 1992)	Imma	4	7.2338 (3)	10.3050 (3)	7.4529 (3)		1.18	0.62	1.903	Magnetic
2O	Na₂NiAlF₇ (Tressaud et al., 1974; Heger, 1973)	Imma	4	7.31 (2)	7.07 (2)	10.04 (2)		1.18	0.603	1.959	Magnetic
2O	Na₂NiCoF₇ (Tressaud et al., 1974; Cosier et al., 1970)	Imma	4	7.40 (2)	7.20 (2)	10.24 (2)		1.18	0.618	1.911	Magnetic
2O	Na₂NiCrF₇ (Hansler & Rudorff, 1970; Laligant, Ferey et al., 1987)	Imma	4	7.183 (1)	10.224 (1)	7.414 (1)		1.18	0.653	1.808	Magnetic
2O	Na₂CoGaF₇ (Koch & Hebecker, 1988)	Imma	4	7.3011 (6)	10.5436 (9)	7.3845 (7)		1.18	0.645	1.829	
2O	Na₂CoInF₇ (Koch & Hebecker, 1988)	Imma	4	7.4032 (6)	10.3892 (8)	7.5302 (9)		1.18	0.745	1.5849	
2O	Na₂CoScF₇ (Koch & Hebecker, 1988)	Imma	4	7.431 (1)	10.546 (1)	7.544 (1)		1.18	0.718	1.645	
2O	Na₂MnTlF₇ (Koch & Hebecker, 1988)	Imma	4	7.371 (1)	10.369 (3)	7.603 (1)		1.18	0.67	1.761	
2O	Na₂NiGaF₇ (Koch & Hebecker, 1988; Dahlke et al., 1998)	Imma	4	7.1805 (7)	10.2433 (9)	7.4256 (7)		1.18	0.655	1.802	
2O	Na₂NiInF₇ (Koch & Hebecker, 1988)	Imma	4	7.3632 (5)	10.3490 (7)	7.5274 (6)		1.18	0.745	1.584	
2O	Na₂NiScF₇ (Koch & Hebecker, 1988)	Imma	4	7.3116 (7)	10.3278 (9)	7.4779 (7)		1.18	0.718	1.645	
2O	Na₂MgTlF₇ (Koch & Hebecker, 1988)	Imma	4	7.3756 (8)	10.418 (1)	7.5496 (8)		1.18	0.695	1.698	
2O	Na₂ZnFeF₇ (Koch & Hebecker, 1988)	Imma	4	7.281 (1)	10.446 (2)	7.459 (1)		1.18	0.645	1.829	
	Na₂ZnGaF₇ (Koch & Hebecker, 1988)	Imma	4	7.2494 (7)	10.3283 (8)	7.3582 (6)		1.18	0.68	1.735	
2O	Na₂ZnInF₇ (Koch & Hebecker, 1988)	Imma	4	7.4077 (6)	10.4759 (9)	7.5732 (6)		1.18	0.77	1.532	
2O	Na₂ZnTlF₇ (Koch & Hebecker, 1988)	Imma	4	7.338 (1)	10.300 (2)	7.539 (1)		1.18	0.705	1.674	
2O	Na₂MgFeF₇ (Pankhurst et al., 1991; Chassain, 1969)	Imma	4	7.49	7.25	10.26		1.18	0.635	1.858	Magnetic
2O	Na₂MgAlF₇ (Byström, 1944; Knop et al., 1982)	Imma	4	7.501 (1)	9.968 (2)	7.285 (1)		1.18	0.618	1.911	
2O	Na₂ZnAlF₇ (Dahlke & Babel, 1994)	Imma	4	7.092 (1)	10.092 (1)	7.337 (1)		1.18	0.6375	1.851	
2O	Ag₂CuMnF₇ (Koch & Hebecker, 1988)	Imma	4	7.5006 (9)	10.5025 (9)	7.6452 (8)		1.28	0.655	1.954	
2O	Ag₂CoAlF₇ (Koch et al., 1982)	Imma	4	7.252	10.16	7.601		1.28	0.603	2.124	
2O	Ag₂CoGaF₇ (Koch et al., 1982)	Imma	4	7.313	10.35	7.678		1.28	0.655	1.954	
2O	Ag₂CoInF₇ (Koch et al., 1982)	Imma	4	7.544	10.72	7.851		1.28	0.745	1.718	
2O	Ag₂CoScF₇ (Koch et al., 1982)	Imma	4	7.497	10.64	7.789		1.28	0.718	1.784	
2O	Ag₂MnAlF₇ (Koch et al., 1982)	Imma	4	7.360	10.32	7.601		1.28	0.593	2.160	
2O	Ag₂MnGaF₇ (Koch et al., 1982)	Imma	4	7.465	10.62	7.787		1.28	0.645	1.986	
2O	Ag₂MnScF₇ (Koch et al., 1982)	Imma	4	7.634	10.78	7.802		1.28	0.708	1.809	
2O	Ag₂NiGaF₇ (Koch et al., 1982)	Imma	4	7.255	10.28	7.650		1.28	0.655	1.954	
2O	Ag₂NiScF₇ (Koch et al., 1982)	Imma	4	7.463	10.54	7.771		1.28	0.718	1.785	
2O	Ag₂MgAlF₇ (Koch et al., 1982)	Imma	4	7.197	10.01	7.571		1.28	0.618	2.073	
2O	Ag₂MgGaF₇ (Koch et al., 1982)	Imma	4	7.257	10.21	7.664		1.28	0.67	1.910	
2O	Ag₂MgInF₇ (Koch et al., 1982)	Imma	4	7.495	10.62	7.832		1.28	0.76	1.684	
2O	Ag₂MgScF₇ (Koch et al., 1982)	Imma	4	7.427	10.52	7.782		1.28	0.733	1.747	
2O	Ag₂CuAlF₇ (Koch et al., 1982)	Imma	4	7.109	10.22	7.684		1.28	0.623	2.056	
2O	Ag₂CuGaF₇ (Koch et al., 1982)	Imma	4	7.200	10.34	7.755		1.28	0.675	1.896	
2O	Ag₂ZnAlF₇ (Koch et al., 1982)	Imma	4	7.237	10.14	7.590		1.28	0.6375	2.008	
2O	Ag₂ZnGaF₇ (Koch et al., 1982)	Imma	4	7.303	10.32	7.688		1.28	0.68	1.882	
2O	Ag₂ZnInF₇ (Koch et al., 1982)	Imma	4	7.531	10.71	7.841		1.28	0.77	1.662	
2O	Ag₂CoCrF₇ (Koch & Hebecker, 1988)	Imma	4	7.349 (1)	10.376 (1)	7.683 (1)		1.28	0.653	1.962	
2O	Ag₂CoFeF₇ (Koch & Hebecker, 1988)	Imma	4	7.3711 (8)	10.437 (1)	7.7145 (8)		1.28	0.62	2.065	
2O	Ag₂MnFeF₇ (Koch & Hebecker, 1988)	Imma	4	7.490 (1)	10.612 (2)	7.731(1)		1.28	0.61	2.098	

Table 5 (continued)

Type		Space group	Z	a (Å)	b (Å)	c (Å)	β (°)	R_A (Å)	R_B (Å)	R_A/R_B	Properties investigated
2O	Ag$_2$MnInF$_7$ (Koch & Hebecker, 1988)	Imma	4	7.6747 (8)	10.856 (1)	7.8641 (7)		1.28	0.735	1.742	
2O	Ag$_2$MgCrF$_7$ (Koch & Hebecker, 1988)	Imma	4	7.2746 (6)	10.3128 (9)	7.7060 (7)		1.28	0.668	1.918	
2O	Ag$_2$MgFeF$_7$ (Koch & Hebecker, 1988)	Imma	4	7.3100 (7)	10.335 (1)	7.6972 (9)		1.28	0.635	2.016	
2O	Ag$_2$MgTlF$_7$ (Koch & Hebecker, 1988)	Imma	4	7.2506 (9)	10.362 (2)	7.497 (1)		1.28	0.695	1.842	
2O	Ag$_2$CuCrF$_7$ (Koch & Hebecker, 1988)	Imma	4	7.2103 (6)	10.454 (1)	7.7871 (8)		1.28	0.673	1.903	
2O	Ag$_2$CuFeF$_7$ (Koch & Hebecker, 1988)	Imma	4	7.2435 (9)	10.474 (2)	7.769 (1)		1.28	0.64	2	
2O	Ag$_2$CuInF$_7$ (Koch & Hebecker, 1988)	Imma	4	7.3461 (6)	10.7501 (9)	7.9098 (6)		1.28	0.765	1.673	
2O	Ag$_2$ZnCrF$_7$ (Koch & Hebecker, 1988)	Imma	4	7.3165 (7)	10.362 (1)	7.6877 (8)		1.28	0.678	1.889	
2O	Ag$_2$ZnFeF$_7$ (Koch & Hebecker, 1988)	Imma	4	7.359 (1)	10.409 (2)	7.706 (1)		1.28	0.645	1.985	
2O	Ag$_2$ZnMnF$_7$ (Koch & Hebecker, 1988)	Imma	4	7.408 (1)	10.503 (1)	7.6972 (9)		1.28	0.66	1.939	
2O	Ag$_2$NiAlF$_7$ (Dance et al., 1974)	Imma	4	7.564 (6)	7.210 (6)	10.139 (15)		1.28	0.603	2.124	Magnetic
2O	Ag$_2$NiCrF$_7$ (Dance et al., 1974)	Imma	4	7.673 (6)	7.305 (6)	10.285 (9)		1.28	0.653	1.962	Magnetic
2O	Ag$_2$NiFeF$_7$ (Dance et al., 1974)	Imma	4	7.692 (6)	7.345 (6)	10.345 (9)		1.28	0.62	2.065	Magnetic
2O	Ag$_2$NiInF$_7$ (Dance et al., 1974)	Imma	4	7.822 (6)	7.499 (6)	10.622 (9)		1.28	0.745	1.718	Magnetic
2O-II	Na$_2$CuInF$_7$ (Ruchaud et al., 1992)	Pmnb	4	7.318	10.602	7.712		1.18	0.765	1.542	Magnetic
2O-II	Na$_2$CuCrF$_7$ (Kummer et al., 1988; Koch & Hebecker, 1985)	Pmnb	4	7.100 (1)	10.338 (1)	7.518 (1)		1.18	0.673	1.755	
2O-II	Na$_2$CuScF$_7$ (Dahlke & Babel, 1994)	Pmnb	4	7.260 (1)	10.534 (1)	7.658 (1)		1.18	0.7375	1.6	
2O-III	Na$_2$NiInF$_7$ (Frenzen et al., 1992)	Pmnb	4	7.356	10.334	7.523		1.18	0.745	1.584	Magnetic
2O-III	Na$_2$MgInF$_7$ (Caramanian et al., 2001)	Pnma	4	10.435 (1)	7.345 (1)	7.533 (1)		1.18	0.76	1.553	Magnetic
2M	Na$_2$CuGaF$_7$ (Ruchaud et al., 1992)	C2/c	8	12.325 (5)	7.318 (1)	12.780 (5)	109.29 (2)	1.18	0.675	1.748	Magnetic
2M and 4M	Na$_2$CuFeF$_7$ (Welsch & Babel, 1992; Yakubovich et al., 1990; Kummer et al., 1988)	C2/c C2/c	8 16	12.46 (1) 12.444 (2)	7.363 (8) 7.343 (1)	12.93 (1) 24.672 (5)	109.36 (7) 99.27 (3)	1.18	0.64	1.844	
3T	Na$_2$MnAlF$_7$ (Koch & Hebecker, 1988)		6	7.2854 (4)		17.844 (1)		1.18	0.593	1.992	
3T	Na$_2$MnInF$_7$ (Koch & Hebecker, 1988)		6	7.6006 (3)		18.617 (1)		1.18	0.735	1.605	
3T	Na$_2$MnScF$_7$ (Koch & Hebecker, 1988)		6	7.5442 (4)		18.479 (1)		1.18	0.708	1.668	
3T	Na$_2$MnGaF$_7$ (Courbion et al., 1988)	P3$_1$21	6	7.421 (3)		18.166 (6)		1.18	0.645	1.829	
3T	Na$_2$MnCrF$_7$ (Courbion et al., 1988)	P3$_1$21	6	7.401 (1)		18.091 (2)		1.18	0.6425	1.837	
3T	Na$_2$MnVF$_7$ (Peschel & Babel, 1997)	P3$_1$21	6	7.467		18.216		1.18	0.655	1.802	
3T	Na$_2$MnFeF$_7$ (Verscharen & Babel, 1978; Cosier et al., 1970; Boireau et al., 1993)	P3$_1$21	6	7.488 (2)		18.257 (6)		1.18	0.61	1.934	Magnetic
3T	Ag$_2$MnInF$_7$ (Koch & Hebecker, 1988)		6	7.751 (1)		18.838 (4)		1.28	0.735	1.741	
4M	Na$_2$CoAlF$_7$ (Boireau et al., 1993; Gravereau et al., 1992)	C2/c	16	12.378 (4)	7.210 (3)	24.019 (9)	99.67 (2)	1.18	0.613	1.927	Magnetic
4M	Na$_2$ZnGaF$_7$ (Dahlke et al., 1998)	C2/c	16	12.519	7.303	24.353	99.74	1.18	0.68	1.735	
4M	Na$_2$ZnFeF$_7$ (Dahlke et al., 1998)	C2/c	16	12.610	7.359	24.538	99.70	1.18	0.645	1.829	
4M	Na$_2$FeVF$_7$ (Peschel et al., 1995)	C2/c	16	12.710 (3)	7.429 (1)	24.716 (5)	100.03 (3)	1.18	0.625	1.888	
4M	Na$_2$CoVF$_7$ (Peschel et al., 1995)	C2/c	16	12.703 (5)	7.391 (3)	24.651 (5)	100.02 (3)	1.18	0.645	1.829	
4M	Na$_2$FeCrF$_7$ (Peschel et al., 1995)	C2/c	16	12.625 (3)	7.391 (1)	24.695 (5)	99.93 (3)	1.18	0.6125	1.927	
4M	Na$_2$Fe$_2$F$_7$ (Yakubovich et al., 1993; Cosier et al., 1970; Tressaud et al., 1974)	C2/c	16	12.676 (3)	7.422 (1)	24.710 (5)	99.97 (3)	1.18	0.58	2.034	Magnetic
4M	Na$_2$CoFeF$_7$ (Welsch & Babel, 1992; Cosier et al., 1970; Tressaud et al., 1974; Boireau et al., 1993)	C2/c	16	12.622 (10)	7.360 (4)	24.516 (20)	99.71 (5)	1.18	0.62	1.903	Magnetic
4M	Na$_2$CoCrF$_7$ (Boireau et al., 1993; Peschel et al., 1995)	C2/c	16	12.578 (3)	7.335 (1)	24.415 (5)	99.64 (3)	1.18	0.653	1.808	Magnetic
4M	Na$_2$FeAlF$_7$ (Dahlke et al., 1998; Tressaud et al., 1974)	C2/c	16	12.426	7.278	24.206	99.99	1.18	0.563	2.098	Magnetic

Table 6
List of weberite oxides with R_A/R_B and the relative ionicity of the A—O bond.

Type		a (Å)	b (Å)	c (Å)	β (°)	R_A (Å)	R_B (Å)	R_A/R_B	$I_A/(I_B + I_A)$	Properties investigated
		Lattice parameters								**Properties**
2O	Ca₂Sb₂O₇ (Bystrom, 1945; Ivanov et al., 1998; Sato et al., 2002; Lin et al., 2006)	7.28 7.3060 7.2900	7.44 7.4627 10.2000	10.18 10.2263 7.4500		1.12	0.6	1.86667	0.60636	Ferroelectric and photocatalytic
2O	Cd₂Sb₂O₇ (Brisse et al., 1972; Bystrom, 1945)	7.21	7.33	10.14		0.9	0.6	1.5	0.56093	
2O	Sr₂Sb₂O₇ (Knop et al., 1980; Groen & Ijdo, 1988; Lin et al., 2006; Sato et al., 2002)	7.452 7.4557 (2) 7.4557	7.687 10.3708 (3) 10.3708	10.381 7.6860 (1) 7.6860		1.26	0.6	2.1	0.61038	Ferroelectric and photocatalytic
2O	Pb₂Sb₂O₇ (Ivanov & Zavodnik, 1990; Ivanov et al., 1998)	7.484 (1) 7.4774	7.857 (1) 7.8549	10.426 (2) 10.4250		1.29	0.6	2.15	0.54792	Ferroelectric
2O	Ca₂Os₂O₇ (Reading et al., 2002; Weller et al., 2003)	7.2104 (2)	10.1211 (3)	7.3813 (2)		1.12	0.575	1.94783	0.55518	Electronic
2O	Sr₂Bi₂O₇ (Knop et al., 1980)	7.70	7.91	10.58		1.26	0.76	1.65789	0.58305	
2O	Ba₂U₂O₇ (Cordfunke & Ijdo, 1988)	8.1665 (15)	11.3081 (21)	8.1943 (16)		1.42	0.76	1.86842	0.5232	
2O	Na₂Te₂O₇ (Knop & Demazeau, 1981)	7.233 (5)	10.104 (7)	7.454 (5)		1.18	0.56	2.10714	0.64905	
2O	Ag₂Te₂O₇ (Klein et al., 2006)	7.266 (2)	10.1430 (9)	7.6021 (17)		1.28	0.56	2.28571	0.60811	
2O	CaPbSb₂O₇ (Ivanov et al., 1998)	7.3577	7.5362	10.3521		1.205	0.6	2.00833	0.59219	Ferroelectric
2O	DyNaSb₂O₇ (Desgardin et al., 1977)	7.26 (6)	7.41 (5)	10.20 (6)		1.1035	0.6	1.83917	0.6051	
2O	GdNaSb₂O₇ (Desgardin et al., 1977)	7.29 (1)	7.47 (0)	10.20 (7)		1.1165	0.6	1.86083	0.60468	
2O	EuNaSb₂O₇ (Desgardin et al., 1977)	7.30 (0)	7.47 (2)	10.21 (4)		1.123	0.6	1.87167	0.6088	
2O	SmNaSb₂O7 (Desgardin et al., 1977)	7.30 (8)	7.45 (7)	10.22 (7)		1.1295	0.6	1.8825	0.60636	
2O	NdNaSb₂O7 (Desgardin et al., 1977)	7.32 (7)	7.49 (2)	10.24 (2)		1.1445	0.6	1.9075	0.60636	
2O	PrNaSb₂O₇ (Desgardin et al., 1977)	7.33 (7)	7.50 (6)	10.25 (5)		1.153	0.6	1.92167	0.58322	
2O	LaNaSb₂O₇ (Desgardin et al., 1977)	7.37 (8)	7.50 (1)	10.28 (8)		1.17	0.6	1.95	0.60594	
2O	KLuSb₂O₇ (Klein et al., 2006; Sych, Kabanova & Andreeva, 1988; Sych, Kabanova, Garbuz & Kovalenko, 1988)	7.23	10.23	7.39		1.2435	0.6	2.0725	0.60759	
2O	KYbSb₂O₇ (Klein et al., 2006; Sych, Kabanova & Andreeva, 1988; Sych, Kabanova, Garbuz & Kovalenko, 1988)	7.24	10.25	7.40		1.2475	0.6	2.07917	0.61077	
2O	KErSb₂O₇ (Klein et al., 2006; Sych, Kabanova & Andreeva, 1988; Sych, Kabanova, Garbuz & Kovalenko, 1988)	7.26	10.25	7.41		1.257	0.6	2.095	0.6088	
2O	KHoSb₂O₇ (Klein et al., 2006; Sych, Kabanova & Andreeva, 1988; Sych, Kabanova, Garbuz & Kovalenko, 1988)	7.26	10.25	7.42		1.2625	0.6	2.10417	0.6092	
2O	KYSb₂O₇ (Klein et al., 2006; Sych, Kabanova & Andreeva, 1988; Sych, Kabanova, Garbuz & Kovalenko, 1988)	7.26	10.25	7.43		1.2645	0.6	2.1075	0.6088	
2O	KYTa₂O₇ (Gade & Chincholkar, 1979)	7.78	10.82	7.50		1.2645	0.64	1.97578	0.5324	
2O	KDyTa₂O₇ (Gade & Chincholkar, 1979)	7.80	10.88	7.70		1.2685	0.64	1.98203	0.53282	
2O	KGdTa₂O₇ (Gade & Chincholkar, 1979)	7.84	10.86	7.72		1.2815	0.64	2.00234	0.5324	
2O	KSmTa₂O₇ (Gade & Chincholkar, 1979)	7.86	10.82	7.76		1.2945	0.64	2.02266	0.53405	
2O	NaDyV₂O₇ (Gade & Chincholkar, 1979)	7.53	10.94	7.44		1.1035	0.54	2.04352	0.53496	
2O	NaGdV₂O₇ (Gade & Chincholkar, 1979)	7.56	10.88	7.46		1.1165	0.54	2.06759	0.54352	
2O	NaSmV₂O₇ (Gade & Chincholkar, 1979)	7.58	10.86	7.48		1.1295	0.54	2.09167	0.54526	
2O	NaNdV₂O₇ (Gade & Chincholkar, 1979)	7.62	10.82	7.50		1.1445	0.54	2.11944	0.54526	
2O	NaSrSbTeO₇ (Burchard & Rudorff, 1979)	Not reported				1.22	0.58	2.10345	0.62891	

Table 6 (continued)

Type		Lattice parameters				R_A (Å)	R_B (Å)	R_A/R_B	$I_A/(I_B + I_A)$	Properties investigated
		a (Å)	b (Å)	c (Å)	β (°)					
$2O$	NaCdSbTeO$_7$ (Burchard & Rudorff, 1979)	Not reported				1.04	0.58	1.7931	0.60778	
$2O$	NdCaSbTeO$_7$ (Burchard & Rudorff, 1979)	Not reported				1.15	0.58	1.9828	0.62694	
$2O$	Na$_{0.5}$Cd$_{1.5}$(Fe$_{0.5}$Te$_{1.5}$)O$_7$ (Burchard & Rudorff, 1979)	7.131	7.317	10.183		1.12	0.5575	2.00897	0.59584	
$2O$	Na$_{0.5}$Ca$_{1.5}$(Fe$_{0.5}$Te$_{1.5}$)O$_7$ (Burchard & Rudorff, 1979)	Not reported				1.135	0.5575	2.0358744	0.626874	
$2O$	Ba$_{0.5}$Ca$_{1.5}$(Fe$_{0.5}$Te$_{1.5}$)O$_7$ (Burchard & Rudorff, 1979)	7.176	7.464	10.140		1.195	0.5725	2.08734	0.627674	
$2M$	CaLa$_{1.5}$Sb$_{1.5}$O$_7$ (Au et al., 2007)	7.5753 (3)	10.6870 (5)	7.5482 (3)	90.346 (3)	1.15	0.7	1.6428571	0.57329	
$2M$	CaPr$_{1.5}$Sb$_{1.5}$O$_7$ (Au et al., 2007)	7.5188 (3)	10.6111 (4)	7.4952 (2)	90.315 (2)	1.1245	0.7	1.6064286	0.569502	
$2M$	CaNd$_{1.5}$Sb$_{1.5}$O$_7$ (Au et al., 2007)	7.5019 (2)	10.5890 (3)	7.4770 (2)	90.298 (2)	1.11175	0.7	1.5882143	0.569502	
$2M$	CaY$_{1.5}$Sb$_{1.5}$O$_7$ (Au et al., 2007)	7.3905 (1)	10.4563 (2)	7.3894 (1)	90.049 (1)	1.04425	0.7	1.4917857	0.55821	
$3T$	Ca$_{1.5}$Mn$_{0.5}$Sb$_2$O$_7$ (Bonazzi & Bindi, 2007)	7.282 (2)		17.604 (4)		1.04	0.6	1.73333	0.59369	
$3T$	Mn$_2$Sb$_2$O$_7$ (Scott, 1990)	7.191		17.402		0.96	0.6	1.6	0.540094	
$3T$	Ca$_{1.92}$Ta$_{1.92}$Nd$_{0.08}$Zr$_{0.08}$O$_7$ (Grey et al., 2003)	7.356 (1)		18.116 (1)		1.11956	0.61728	1.8136988	0.529853	
$3T$	Ca$_2$Ta$_2$O$_7$ (Cava et al., 1998; Grey et al., 1999)	7.355 (1)		18.09 (1)		1.12	0.64	1.75	0.52985	Dielectric
$4M$	Ca$_{1.92}$Ta$_{1.92}$Nd$_{0.08}$Zr$_{0.08}$O$_7$ (Grey et al., 2003)	12.761 (1)	7.358 (1)	24.565 (1)	100.17	1.12	0.64	1.75	0.52922	
$5M$	Ca$_{1.8}$Ta$_{1.8}$Sm$_{0.24}$Ti$_{0.17}$O$_7$ (Grey & Roth, 2000)	12.763 (1)	7.130 (1)	30.190 (1)	94.09 (1)	1.13635	0.62743	1.81113	0.52523	
$5M$	Ca$_2$Ta$_{1.8}$Nb$_{0.2}$O$_7$ (Grey et al., 2001)	12.749 (1)	7.347 (1)	30.23 (1)	94.23 (1)	1.12	0.64	1.75	0.52866	Dielectric
$6M$	Ca$_2$Ta$_2$O$_7$ (Grey et al., 1999)	7.348 (3)	12.727 (3)	36.44 (5)	95.9 (1)	1.12	0.64	1.75	0.52985	
$6T$	Ca$_{1.89}$Ta$_{1.86}$Sm$_{0.16}$Ti$_{0.1}$O$_7$ (Grey & Roth, 2000)	7.353 (1)		36.264 (1)		1.1792	0.63505	1.85686	0.52649	
$7M$	Ca$_2$Ta$_{1.9}$Nb$_{0.1}$O$_7$ (Grey et al., 2001)	12.714 (1)	7.370 (1)	42.45 (1)	95.75 (1)	1.12	0.64	1.75	0.52925	Dielectric
$8O$	Ca$_2$Ta$_2$O$_7$ (Ebbinghaus et al., 2005)	7.3690 (2)	12.7296 (3)	48.263 (1)		1.12	0.64	1.75	0.52985	Dielectric and optical

R is the ionic radius from Shannon (1976), χ is the electronegativity from Allred & Rochow (1958), I is the bond ionicity.

elongated perpendicular to the B-1 chains) in CuF$_6$ octahedra leads to the lowering of symmetry, while maintaining the orthorhombic lattice. The space group is reduced to $Pmnb$, a subgroup of $Imma$ (Yakubovich et al., 1993). Another case of losing I-centering symmetry happens when the ionic radius of B-2 is larger than that of B-1. In a classic $2O$ weberite structure the ionic radius of B-2 is equal to or smaller than that of B-1. When a larger B-2 ion appears in a weberite compound, the anions, which are shared by two B-1 octahedral neighbors, distort toward B-2 ions. As a result, the A-2 ions cannot hold eight-coordination and change to seven-coordination. The B-2 ion keeps octahedral coordination with a seventh anion relatively close to it. As in the case of Na$_2$NiInF$_7$, the distance between the distorted anion and B-2 (In^{3+}) is only 1.3 times larger than the shortest In—F bond length in B-2 octahedra (Frenzen et al., 1992). In a $2O$ weberite structure, the ratio of the two distances is higher, such as 1.97 in Na$_2$MgAlF$_7$ or 1.83 in Ca$_2$Os$_2$O$_7$ (Wyckoff, 1963; Reading et al., 2002). The distortion of the anion excludes the I-centering of the structure and results in the space group $Pnmb$ (Yakubovich et al., 1993). The notation of $2O$-II and $2O$-III is used for the first and the second condition, respectively.

One extreme case for $2O$-III is Ln$_2$(B,Ln)O$_7$ (or Ln$_3$BO$_7$, where Ln^{3+} is a rare-earth element, and B is Os^{5+}, Re^{5+}, Ru^{5+}, Re^{5+}, Mo^{5+}, Ir^{5+}, Sb^{5+}, Nb^{5+} or Ta^{5+}). B-2 ions are the same as A ions. As a result, the B-2 sites and A-2 sites are indistinguishable. The structure has an arrangement of BO$_6$–LnO$_8$

layers (much like weberites), but a different cation configuration with VII coordination between the layers (Fig. 11). Due to the fact that this type of structure does not maintain the three-dimensional BO$_6$ octahedral network, it is considered a weberite-type structure rather than the weberite structure, or sometimes it is reported as a La$_3$NbO$_7$-type structure (Rossell, 1979; Allpress & Rossell, 1979; Rooksby & White, 1964; Abe et al., 2004, 2006; Cai & Nino, 2007; Cai et al., 2007; Wakeshima et al., 2004; Groen et al., 1987; Wakeshima & Hinatsu, 2006; Nishimine et al., 2007; Gemmill et al., 2007; Khalifah et al., 1999, 2000; Wiss et al., 2000; Bontchev et al., 2000; Harada & Hinatsu, 2001; Harada et al., 2001; Nishimine et al., 2005; Gemmill et al., 2004, 2005; Vanberkel & Ijdo, 1986; Kahnharari et al., 1995; Wltschek et al., 1996; Greedan et al., 1997; Lam et al., 2002; Plaisier et al., 2002; Lam et al., 2003; Barrier & Gougeon, 2003; Hinatsu et al., 2004; Vente & Ijdo, 1991). Table 7 lists examples of Ln$_3$BO$_7$ and their properties that have been investigated. Details on the dielectric properties of Ln$_3$NbO$_7$ have been reported and will be covered in §3.2.2.

There is a special type of weberite ($B^{+2}B^{+3}$F$_5$·2H$_2$O) named inverse weberite (please see Table 7 for examples). In this structure A cations are missing. In order to maintain charge neutrality, two H$_2$O molecules take the place of two F$^-$ ions. This structure has the same characteristic B octahedral network, just like the $2O$ weberite structure. The space group and Wyckoff positions of B cations and anions are the same as

feature articles

in the $2O$ weberite. However, B^{2+} ions take B-2 sites while B^{3+} cations lie at B-1 sites in this structure, which is opposite to the classic weberite structure (Laligant, Calage *et al.*, 1986; Laligant, Leblanc *et al.*, 1986; Laligant, Pannetier *et al.*, 1986; Laligant, Pannetier *et al.*, 1987; Weil & Werner, 2001; Leroux *et al.*, 1995; Subramanian *et al.*, 2006).

The investigation of $Na_2B^{2+}B^{3+}F_7$ weberites indicates that the resulting structure type is determined by the size of the B^{2+}

cations. With increasing ionic radius of B^{2+}, the structure changes from $2O$ to $2M$, $4M$ and to $3T$, gradually (Yakubovich *et al.*, 1993). As for oxide weberites, it is clear that the A cation still plays an important role, for example, $2O$ $Ca_2Sb_2O_7$, $3T$ $Ca_{1.5}Mn_{0.5}Sb_2O_7$ and $3T$ $Mn_2Sb_2O_7$ (Ivanov *et al.*, 1998; Bonazzi & Bindi, 2007; Scott, 1990; Butler *et al.*, 1950; Bystrom, 1945). The occurrence of the monoclinic and trigonal variants may be closely related to the ionic radius ratio of the A and B cations. However, due to the limited number of compounds reported in each weberite-like structure, it is difficult to define the factors that determine when the variants occur.

As discussed before, the unpaired vertex (terminal anions) of B-2 octahedra are in *trans* configurations in $2O$ weberites. The trigonal and monoclinic variants produce another type of B-2 octahedra with the *cis* configuration (see Figs. 2b and c). Grey and co-workers (Grey & Roth, 2000; Grey *et al.*, 2003) figured out that the relative position of the terminal anions is a characteristic of weberite polytypes. In $2M$ and $3T$ polytypes *cis-B2* are only in A_3B layers, while *trans-B2* are only in AB_3 layers (Grey *et al.*, 2003; Yakubovich *et al.*, 1993). The $4M$ and $6T$ weberites have alternative *cis* and *trans* configurations in successive A_3B layers (Grey & Roth, 2000; Grey *et al.*, 2003).

Several research groups (Yakubovich *et al.*, 1993, 1990; Dahlke *et al.*, 1998; Verscharen & Babel, 1978; Welsch & Babel, 1992) proposed that the formation of B-1 chains is a characteristic of $Na_2B^{2+}B^{3+}F_7$ weberite polytypes. The detailed description about the different stacking sequence and the orientation of B-1 chains in $2O$, $2M$, $3T$ and $4M$ variants has been reported by Yakubovich *et al.* (1993). Here, the discussion is expanded to include all $2O$, $2M$, $3T$, $4M$, $5M$, $6M$, $6T$, $7M$ and $8O$ variants. There are three different orientations for B-1 chains: type α, type β and type γ. These three orientations are correlated with each other by a threefold rotation.
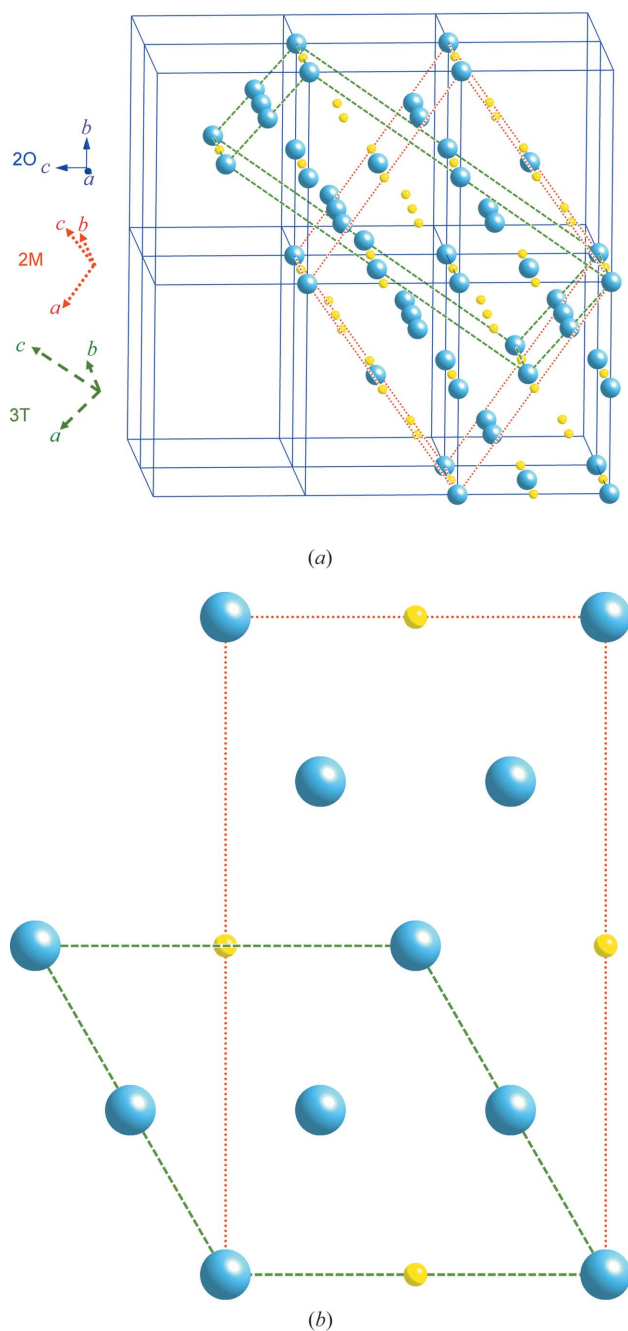

Figure 10
(a) Relationship between $2O$, $2M$ and $3T$ weberites (origin at the $A2$ site); large spheres: A ions; small spheres: B ions; blue solid lines: multiple unit cells of $2O$; red dotted lines: the unit cell of $2M$; green dashed lines: the unit cell of $3T$. (b) (001) plane of $3T$ (green dashed lines) and $2M$ [red dotted lines, also indicating (011) of $2O$].
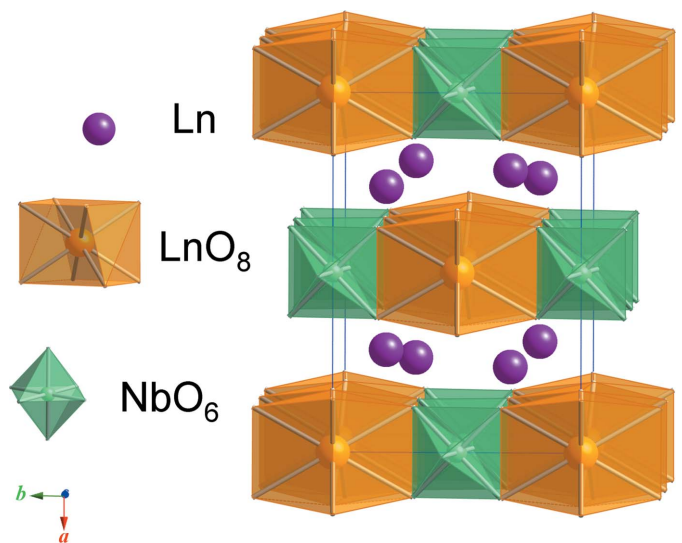

Figure 11
Weberite-type Ln_3BO_7, viewed in the [0.05, 0.05, 1] direction. The layers of LnO_8 and BO_6 lines are parallel to the (001) plane. Between the layers are Ln with a coordination number of 7.

Table 7
Examples of weberite-type Ln_3BO_7 and inverse weberites.

Type	Compounds	Space group	Z	Lattice parameters			Properties investigated
				a (Å)	b (Å)	c (Å)	
Weberite type	La$_3$NbO$_7$ (Abe *et al.*, 2004, 2006; Allpress & Rossell, 1979)	*Cmcm*	4	11.167 (1)	7.629 (1)	7.753 (1)	Dielectric and photocatalytic
Weberite type	La$_3$TaO$_7$ (Allpress & Rossell, 1979; Abe *et al.*, 2004, 2006)	*Cmcm*	4	11.1863 (4)	7.6152 (3)	7.7556 (3)	Catalytic and magnetic
Weberite type	Pr$_3$NbO$_7$ (Vente *et al.*, 1994)	*Cmcm*	4	10.959 (1)	7.5240 (7)	7.6676 (7)	Magnetic
Weberite type	Pr$_3$TaO$_7$ (Vente *et al.*, 1994)	*Cmcm*	4	10.973 (1)	7.5230 (7)	7.6721 (7)	Magnetic
Weberite type	Nd$_3$NbO$_7$ (Cai *et al.*, 2007; Allpress & Rossell, 1979)	*Cmcm*	4	10.905 (2)	7.517 (2)	7.624 (1)	Dielectric
Weberite type	Gd$_3$NbO$_7$ (Cai *et al.*, 2007; Allpress & Rossell, 1979; Astafyev *et al.*, 1985)	*C*222$_1$	4	10.610 (1)	7.521 (1)	7.550 (1)	Dielectric
Weberite type	Gd$_3$TaO$_7$ (Wakeshima *et al.*, 2004)	*C*221$_1$	4	10.6259 (4)	7.5234 (3)	7.5446 (3)	Magnetic
Weberite type	Dy$_3$TaO$_7$ (Wakeshima *et al.*, 2004)	*C*222$_1$	4	10.5332 (3)	7.4447 (2)	7.4816 (2)	Magnetic
Weberite type	Ho$_3$TaO$_7$ (Wakeshima *et al.*, 2004)	*C*222$_1$	4	10.4873 (4)	7.4292 (3)	7.4499 (3)	Magnetic
Inverse	Fe$_2$F$_5$(H$_2$O)$_2$ (Laligant, Pannetier *et al.*, 1986; Greneche *et al.*, 1988; Hall *et al.*, 1977)	*Imma*	4	7.447 (1)	10.8623 (2)	6.652 (1)	Magnetic
Inverse	ZnFeF$_5$(H$_2$O)$_2$ (Laligant, Calage *et al.*, 1986)	*Imma*	4	7.475 (1)	10.766 (1)	6.594 (1)	Magnetic
Inverse	MnFeF$_5$(H$_2$O)$_2$ (Laligant, Calage *et al.*, 1986; Laligant, Pannetier *et al.*, 1987; Greneche *et al.*, 1988)	*Imma*	4	7.5635 (2)	10.901 (1)	6.7319 (3)	Magnetic
Inverse	MnAlF$_5$(H$_2$O)$_2$ (Subramanian *et al.*, 2006)	*Imma*	4	7.229 (2)	10.487 (4)	6.816 (2)	
Inverse	MgAlF$_5$(H$_2$O)$_2$ (Subramanian *et al.*, 2006; Weil & Werner, 2001)	*Imma*	4	7.057 (2)	10.125 (4)	6.798 (2)	Electrical resistivity
Inverse	MnVF$_5$(H$_2$O)$_2$ (Subramanian *et al.*, 2006; Leroux *et al.*, 1995)	*Imma*	4	7.607 (2)	10.912 (4)	6.728 (2)	Magnetic

For 2O weberites (including 2O-II and 2O-III), the stacking sequence of B-1 chains is $\alpha\alpha\alpha\ldots$ (the orientation is parallel to the [100] direction). The same applies for pseudo-2O NaCu$_3$F7 and CaLn$_{1.5}$Sb$_{1.5}$O$_7$ (Ln = La, Pr, Nd and Y), special cases of 2M (Renaudin *et al.*, 1988; Au *et al.*, 2007). The directions of the B-1 chains for 2M (except NaCu$_3$F$_7$ and CaLn$_{1.5}$Sb$_{1.5}$O$_7$) and 4M weberites are either nearly parallel to [110] (type β) or [$\bar{1}$10] (type γ). The stacking array for 2M is $\beta\gamma\beta\gamma$, while it is $\beta\beta\gamma\gamma\beta\beta\gamma\gamma$ for the 4M polytype. As for 3T and 6T, the directions of the B-1 chains are nearly parallel to [010], [100] or [110]. The sequence of B-1 chains is $\alpha\beta\gamma$ in 3T and $\alpha\alpha\beta\beta\gamma\gamma\alpha\alpha\beta\gamma\gamma$ in 6T weberites.

It is important to note that the close-packed cation layers are stacked the same as f.c.c. (face-centered cubic: cubic stacking in which the stacking sequence is $ABCABC\ldots$) in 2O, 2M, 3T, 4M and 6T polytypes. The cation layers in 5M, 6M, 7M and 8O polytypes (Ca$_2$Ta$_2$O$_7$-based compounds) are a mixture of cubic stacking and hexagonal stacking. The hexagonal stacking layers act as mirror glide planes for the cations, for example, the stacking sequence of 5M is $ABC\underline{A}CBA\underline{C}AB$ in a unit cell (the underline letters indicate a hexagonal stacking; Grey *et al.*, 1999, 2001). Therefore, 5M, 6M, 7M and 8O polytypes are not pure weberite. The weberite blocks are separated by h-stacking layers. A simpler approach is to describe the stacking of c as cubic and h as hexagonal. The stacking sequence is $ccchcchcc$ for 5M [simplified as (3c)h(3c)h(2c), the integers indicating the number of c stacking layers], (5c)h(5c)h for 6M, (5c)h(7c)h for 7M and (4c)h(7c)h(3c) for 8O (Ebbinghaus *et al.*, 2005; Grey *et al.*,

1999, 2001, 2003; Grey & Roth, 2000). There are several structural features resulting from the introduction of h stacking:

(i) h stacking only occurs in the CaTa$_3$ cation layers;

(ii) h stacking causes the appearance of B-3 octahedra on the CaTa$_3$ cation layers and the neighboring Ca$_3$Ta cation layers, which have only one unpaired vertex (B-1 octahedra have no unpaired vertex and B-2 have two);

(iii) in h stacking layers B-3 chains are formed, but no B-1 chains.

In these cases type α is nearly parallel to [100] for 8O or [010] for 5M and 7M. Type β is nearly parallel to [110] and type γ is nearly parallel to [$\bar{1}$10]. The directions of the B chains are $\beta\beta\underline{\alpha}\gamma\gamma$ for 5M, $\gamma\beta\gamma\beta\gamma\beta$ for 6M, $\gamma\underline{\alpha}\gamma\alpha\beta\underline{\alpha}\beta$ for 7M and $\alpha\underline{\beta}\underline{\alpha}\gamma\alpha\beta\underline{\alpha}\gamma$ for 8O (B-3 chains are underlined). In summary, the stacking sequence of B chains changes with different weberite variants (see Fig. 12) and the formation of B chains is a characteristic of all weberites.

2.4. Stability field

Both pyrochlores and weberites have BX_6 octahedral networks. Owing to the fact that B-2 octahedra have two unpaired vertices, the BX_6 octahedral network in weberite is typically less compact. Therefore, weberite has more potential to permit larger radii of A ions. Fig. 13 shows a diagram of R_A versus R_B for 159 pyrochlore oxides and 131 weberite compounds (83 weberite fluorides and 48 weberite oxides, see Tables 5 and 6 for a complete list and references). The 159

pyrochlore oxides are taken from two articles (Subramanian *et al.*, 1983; Isupov, 2000). Fig. 13 indicates that the majority of pyrochlores have R_A ranging from 0.97 to 1.13 Å, while most weberites have R_A values ranging from 1.10 to 1.30 Å.

Weberite $Ba_2U_2O_7$ has the highest R_A value of 1.42 Å (Cordfunke & Ijdo, 1988; Shannon, 1976). This clearly shows that larger R_A values prefer the formation of the weberite (Brisse *et al.*, 1972). The ratio of R_A/R_B for the weberite is
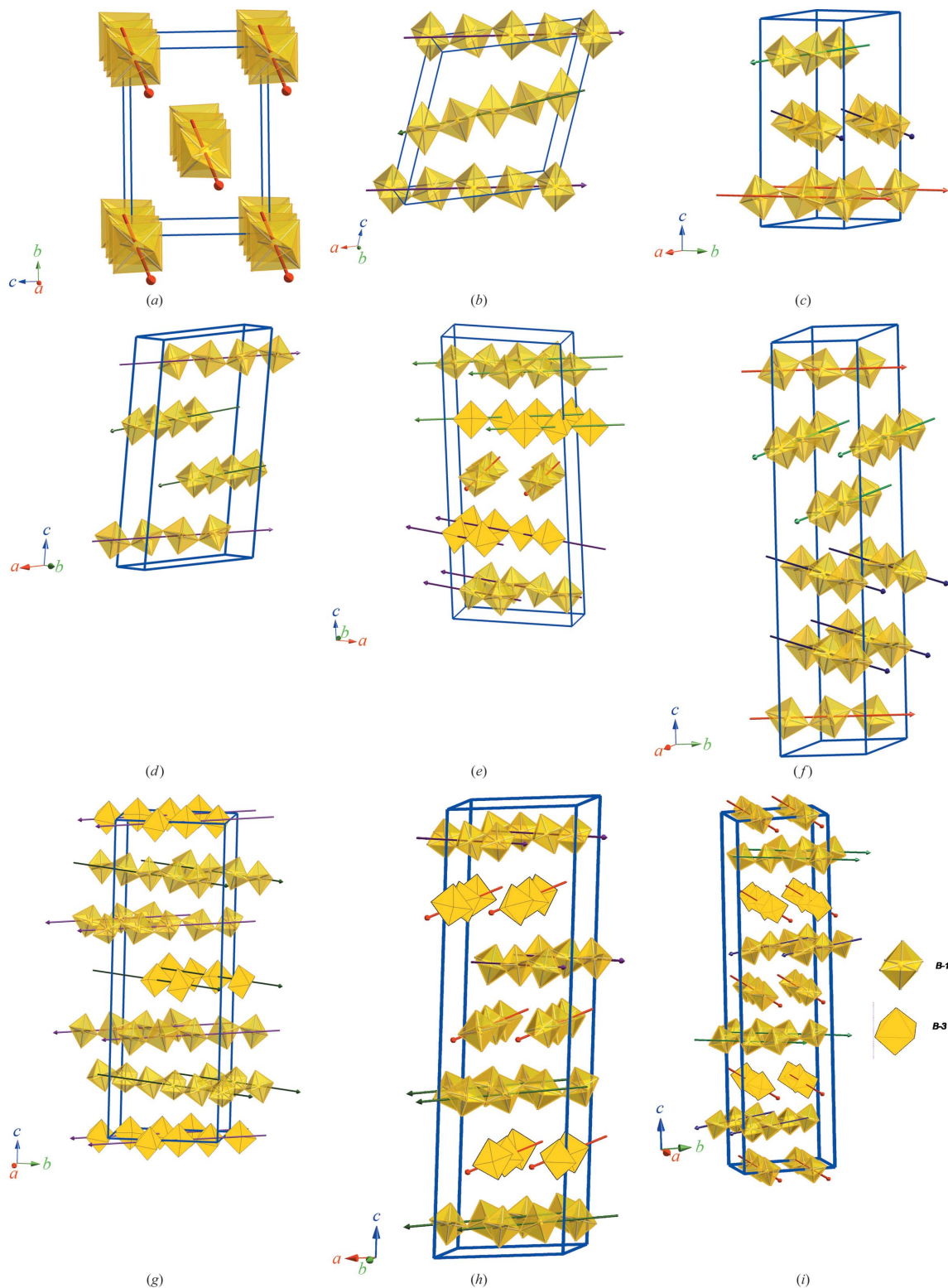

Figure 12
B chains in different weberite-like structures. The vectors across the octahedra indicate the orientations of the B chains. (a) 2O, (b) 2M, (c) 3T, (d) 4M, (e) 5M, (f) 6T, (g) 6M, (h) 7M and (i) 8O.

between 1.5 and 2. The two end-members are $Cd_2Sb_2O_7$ and $Ag_2Te_2O_7$. However, the range of R_A/R_B for weberite greatly overlaps with the stability field for pyrochlore: 1.46–1.8 for $A_2^{3+}B_2^{4+}O_7$ and 1.4–2.2 for $A_2^{2+}B_2^{5+}O_7$ (Subramanian *et al.*, 1983). Therefore, the ionic radius ratio is not the only determining factor in the structural stability.

Electronegativity (χ) is another important factor in the field of existence, because the formation of weberites is closely related to the covalent character of the bonds (Sych, Kabanova, Garbuz *et al.*, 1988; Lopatin *et al.*, 1985; Weller *et al.*, 2003; Burchard & Rudorff, 1979). Weller *et al.* (2003) used only χ_A and χ_B to picture the stability field of the weberite, but their study only included a limited number of compounds. Lopatin *et al.* (1982, 1985) successfully utilized χ_A and R_A/R_B to distinguish pyrochlores and weberites, and χ_B and R_A/R_B to determine the different regions of the weberite and the layered perovskite. They chose Allred–Rochow (Allred & Rochow, 1958) electronegativities (which were completed by Little & Jones, 1960) because Allred–Rochow electronegativities are more precise when measuring the degree of covalent character of the bonds. Sych *et al.* (Sych, Kabanova, Garbuz *et al.*, 1988) introduced R_A/R_B *versus* the relative ionicity of the A—O bond, which is the ratio of the ionicity of the A—O bond to the sum of the ionicity of the A—O and B—O bonds. The ionicity of the A—O bond is calculated as

$$I_{A-O} = 1 - \exp[-0.25(\chi_A - \chi_O)^2]. \qquad (4)$$

They used the electronegativities for the crystalline state calculated by Batanov (1975). The advantage of relative ionicity is that it contains the information for both A—O and B—O bonds. Therefore, the relative ionicity of A—O *versus* R_A/R_B is used to determine the stability field in this study, as shown in Fig. 14. Here, the electronegativities of Allred–Rochow (Allred & Rochow, 1958) and Little–Jones (Little & Jones, 1960) were used in calculating the ionicity. In Fig. 14(a) there is no obvious separation between weberites and pyrochlores. The reason for this may be that both $A_2^{2+}B_2^{5+}O_7$ and $A_2^{3+}B_2^{4+}O_7$ pyrochlore compounds are plotted. There are very
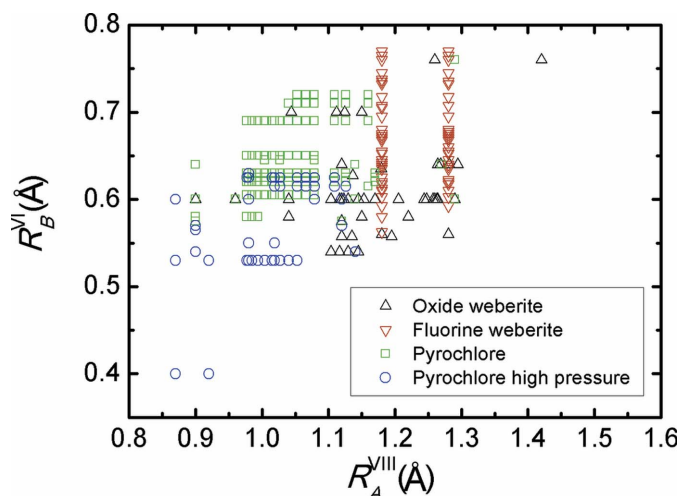
few, if any, $A_2^{3+}B_2^{4+}O_7$ weberites reported. Most weberites are $A_2^{2+}B_2^{5+}O_7$ or $(A, A')_2^{2+}(B, B')_2^{5+}O_7$ and several $A_2^{1+}B_2^{6+}O_7$ ($Na_2Te_2O_7$ and $Ag_2Te_2O_7$). The inclusion of $A_2^{3+}B_2^{4+}O_7$, particularly high-pressure phases, complicates the stability field, therefore, Fig. 14(b) only contains $A_2^{2+}B_2^{5+}O_7$, $(A, A')_2^{2+}(B, B')_2^{5+}O_7$ compounds $Na_2Te_2O_7$ and $Ag_2Te_2O_7$ (all weberites points in Fig. 14b are listed in Table 6). Observing the plotted data in Fig. 14(b), there is a clear separation between weberites and pyrochlores. The dashed line is for visual effect – above the line is the weberite region. Weberites prefer a higher ratio of $I_{A-O}/(I_{A-O} + I_{B-O})$ and a higher ratio of R_A/R_B than pyrochlores.

It is worth mentioning four specific compounds: $Cd_2Sb_2O_7$ ($R_{Cd^{2+}} = 0.9$ Å) in the pyrochlore region, and $Ca_2Sb_2O_7$, Ca_2Os_2O7 ($R_{Ca^{2+}} = 1.12$ Å) and $Pb_2Sb_2O_7$ ($R_{Pb^{2+}} = 1.29$ Å) in the weberite region (Shannon, 1976). A high-pressure study has been performed on the first three compounds to investigate the transformation of the pyrochlore and weberite phases. $Cd_2Sb_2O_7$ can form a metastable phase of weberite, which can be fully converted to pyrochlore under high pressure. $Ca_2Sb_2O_7$ weberite is more stable than $Cd_2Sb_2O_7$ weberite. The same high-pressure condition only results in mixed phases of $Ca_2Sb_2O_7$ pyrochlore and weberite (Knop *et al.*, 1980). At one atmosphere, $Ca_2Sb_2O_7$ crystallizes as a pyrochlore below 973 K, above which it transforms to a weberite (Brisse *et al.*, 1972). Meanwhile, $Ca_2Os_2O_7$ weberite is stable and the synthesis of pyrochlore $Ca_2Os_2O_7$ under pressure leads to calcium-deficient $Ca_{1.7}Os_2O_7$ (Reading *et al.*, 2002; Weller *et al.*, 2003). The reported crystal structure of $Pb_2Sb_2O_7$ also strongly depends on the synthesis conditions. Low-temperature firing or wet chemical synthesis resulted in a

Figure 13
Summary of R_A versus R_B for weberites (including oxide and fluorine) and pyrochlore oxides.
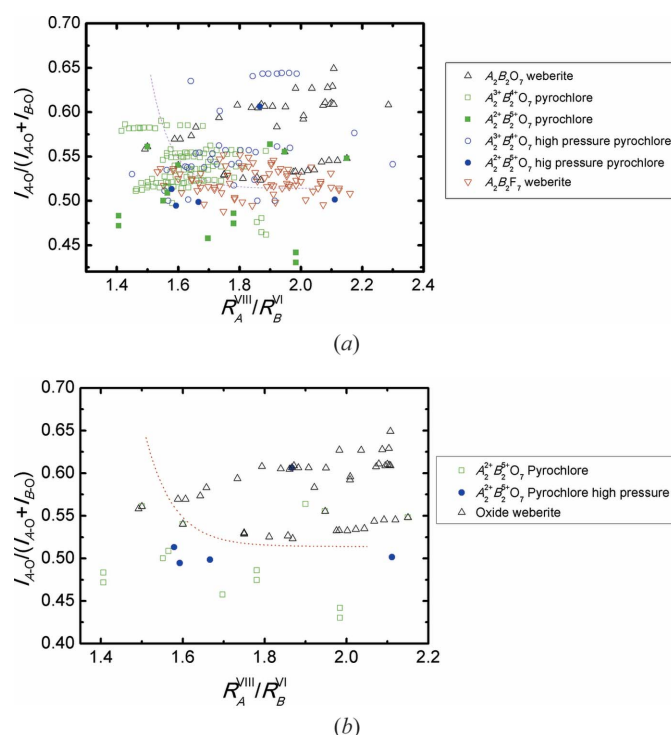

Figure 14
Stability field for weberite.

cubic pyrochlore phase. The cubic phase was metastable and readily transformed into weberite or rhombohedrally distorted pyrochlore (Ivanov *et al.*, 1998; Brisse *et al.*, 1972). These four compounds can crystallize as different polymorphs depending on the processing history, as presented in Fig. 14(*b*). It is worth noting that although the ionic radii ratio and bond ionicity are two major factors, there may be some additional crystallochemical characteristics or parameters that play a role in determining the prevalence of weberite over pyrochlore or *vice versa*. It would be interesting to perform some computational calculations (*e.g.* density functional theory) to shed light on the comparative lattice energy and stability field of pyrochlore and weberite.

3. Interesting properties and potential applications

For fluorine-based weberites, the magnetic properties attract most of the attention. The triangular network formed by B^{2+} and B^{3+} cations in the HTB-like planes generally support three different magnetically ordered systems:

(i) the diamagnetic B^{3+} ions separate linear chains of paramagnetic B^{2+} ions, for example, antiferromagnetic Na_2NiAlF_7, Na_2FeAlF_7 and Na_2NiInF_7 (Frenzen *et al.*, 1992; Heger, 1973);

(ii) both B^{2+} and B^{3+} are paramagnetic ions, like ferromagnetic Na_2NiFeF_7 and antiferromagnetic Na_2NiCrF_7 (Laligant *et al.*, 1989; Thompson *et al.*, 1992; Heger, 1973; Frenzen *et al.*, 1992);

(iii) diamagnetic B^{2+} forming linear chains which isolate the paramagnetic B^{3+} such as antiferromagnetic Na_2MgFeF_7 (Pankhurst *et al.*, 1991).

As for weberite oxide, various properties have been investigated including the photocatalytic properies (Abe *et al.*, 2004, 2006; Sato *et al.*, 2002; Lin *et al.*, 2006), the resistivity of $Ca_2Os_2O_7$ weberite (Reading *et al.*, 2002), magnetic properties (Khalifah *et al.*, 1999; Wakeshima *et al.*, 2004; Wakeshima & Hinatsu, 2006), ferroelectric properties (Ivanov *et al.*, 1998; Astafev *et al.*, 1985) and dielectric properties (Cai & Nino, 2007; Cava *et al.*, 1998; Grey *et al.*, 2001). The interest in the properties is first due to the fact that the weberite structure is considered more favorable for the realisation of a ferroelectric state than the pyrochlore structure (Astafev *et al.*, 1985). The Sb-based compounds are the most investigated weberites for ferroelectric properties. Ten years ago, Cava *et al.* (1998) found that the temperature coefficients of the dielectric constant ($TC\varepsilon_r$) of the $Ca_2Ta_2O_7$–$Ca_2Nb_2O_7$ system can be close to zero. A series of investigations on $Ca_2Ta_2O_7$-based weberites have followed (Grey *et al.*, 1999, 2001, 2003; Grey & Roth, 2000; Ebbinghaus *et al.*, 2005). Ln_3BO_7 (where Ln = rare-earth elements and *B* is Nb or Ta) are also interesting weberite-type compounds. The crystal structure is related to the ionic radius of Ln^{3+}, which provides a stage for the study of structure-dielectric properties relationships. This section will focus on the ferroelectric properties and dielectric properties of weberite oxides.

3.1. Ferroelectric properties

$A_2Sb_2O_7$ (A = Ca^{2+}, Pb^{2+} and Sr^{2+}) are perhaps the most studied weberites owing to their ferroelectric properties. Second-harmonic generation and heat-capacity measurements indicated a possible ferroelectric phase transition in $Pb_2Sb_2O_7$. Dielectric constants showed a thermal hysteresis around the Curie temperature (T_c) in $Pb_2Sb_2O_7$ (Astafev *et al.*, 1985; Milyan & Semrad, 2005). Single-crystal X-ray and powder neutron diffraction were performed in detailed crystallographic studies (Ivanov & Zavodnik, 1990; Astafev *et al.*, 1985). Below T_c, there is a slight distortion from a centrosymmetric structure and ionic displacements cause spontaneous polarization in this structure. The results indicated a non-centrosymmetric (space group *I2cm*) to centrosymmetric (space group *Imam*, another setting of *Imma*) phase transition (Astafev *et al.*, 1985; Ivanov *et al.*, 1998; Ivanov & Zavodnik, 1990). T_c depends on the A cation: 510 K for $Pb_2Sb_2O_7$, 110 K for $Ca_2Sb_2O_7$ and 90 K for $Sr_2Sb_2O_7$. The substitution of Ca by Pb in $Ca_2Sb_2O_7$ causes a shift of T_c towards a higher temperature: 200 K for $CaPbSb_2O_7$ weberite. Therefore, the A sublattice seems more likely to be the ferroelectrically active one.

It is worth noting that $Pb_2Sb_2O_7$ can also form rhombohedrally distorted pyrochlore (Brisse *et al.*, 1972). The pyrochlore phase is paraelectric even at room temperature. Actually, Pb_2Sb_2O7 weberite has a higher T_c than most Pb-based pyrochlores. These facts may serve as evidence that the weberite structure is more suitable for the appearance of the ferroelectric state (Astafev *et al.*, 1985; Isupov, 2000).

3.2. Dielectric properties

3.2.1. $Ca_2Ta_2O_7$-based compounds. According to Grey and co-workers (Grey *et al.*, 1999) the structure of pure $Ca_2Ta_2O_7$ is 3*T* weberite up to 1673 K, where it transforms to the 7*M* polytype. The structure can be easily modified by doping and different synthesis routines (Grey *et al.*, 1999, 2001, 2003; Grey & Roth, 2000; Ebbinghaus *et al.*, 2005). One of the most interesting dielectric properties of $Ca_2Ta_2O_7$ is that the temperature coefficient of the dielectric constant ($TC\varepsilon_r$) is 0 when mixing with 18 mol% of $Ca_2Nb_2O_7$, meeting the requirement for the application of microwave dielectrics (Cava *et al.*, 1998). $TC\varepsilon_r \simeq 0$ can be easily understood because $TC\varepsilon_r$ is negative for $Ca_2Ta_2O_7$ (-444 p.p.m. K^{-1} at 295 K) and positive for $Ca_2Nb_2O_7$ (231 p.p.m. K^{-1} at 295 K). Extensive studies on the structure of the $(1-x)Ca_2Ta_2O_{7-x}Ca_2Nb_2O_7$ system have been performed by powder and single-crystal X-ray diffraction, and powder neutron diffraction (Grey *et al.*, 2001). The system forms 7*M* weberite solid solutions up to x = 0.1 and $Ca_2Nb_2O_7$-type solid solutions from x = 0.2–1. When x = 0.1, the structure transforms into 5*M*. The solubility limit is reached when the substitution of $Ca_2Nb_2O_7$ increases to 15 mol% and $Ca_2Nb_2O_7$ forms as a second phase. The presence of $Ca_2Nb_2O_7$ thus results in $TC\varepsilon_r$ compensation, making it approximately zero.

Another interesting aspect is that most of the $(1-x)Ca_2Ta_2O_{7-x}Ca_2Nb_2O_7$ compounds have higher dielec-

Table 8
Structural comparison of three weberite-type structures (Allpress & Rossell, 1979; Rossell, 1979).

	La$_3$NbO$_7$	Nd$_3$NbO$_7$	Gd$_3$NbO$_7$
$\Delta d_{Ln-O}/(d_{Ln-O})_{av}$ in LnO$_8$ cube (%)	13.33	7.14	13.06
Deviation of O—Ln—O angle from perfect cube (°)	−9.87–6.46	−2.37–2.47	−5.77–8.88
$\Delta d_{Nb-O}/(d_{Nb-O})_{av}$ in NbO$_6$ octahedra (%)	1.64	0.41	4.86
Deviation of O—Nb—O angle from perfect octahedra	−1.58–1.58	0.27–0.42	−5.63–5.63

d_{Ln-O} and d_{Nb-O} represents the bond length between Ln^{3+} and O^{2-} and the bond length between Nb^{5+} and O^{2-}, respectively. Δd_{Ln-O} means the difference of longest and shortest bond length between Ln^{3+} and O^{2-} in LnO$_8$ distorted cubes. Δd_{Nb-O} is the difference of the longest and shortest bond length between Nb^{5+} and O^{2-} in NbO$_6$ distorted octahedra. $(d_{Ln-O})_{av}$ is the average bond length between Ln^{3+} and O^{2-} in LnO$_8$ distorted cubes. $(d_{Nb-O})_{av}$ is the average bond length between Nb^{5+} and O^{2-} in NbO$_6$ distorted octahedra.

tric constants (above 30) than pure Ca$_2$Ta$_2$O$_7$ and Ca$_2$Nb$_2$O$_7$ at 1 MHz (Cava *et al.*, 1998). However, another set of published dielectric constants of 5*M* Ca$_2$Ta$_{1.8}$Nb$_{0.2}$O$_7$ and 7*M* Ca$_2$Ta$_{1.9}$Nb$_{0.1}$O$_7$ are approximately 18 and 20 at 1 MHz, respectively, which are lower than the previous publication (Grey *et al.*, 2001). It is not clear what causes the discrepancy in dielectric constant measurement. It may be due to different firing conditions and measurement methods. Dielectric properties at radio frequency have also been investigated. The dielectric constants of 3*T* Ca$_{1.6}$Nd$_{0.4}$Ta$_{1.6}$Zr$_{0.4}$O$_7$, 5*M* Ca$_2$Ta$_{1.8}$Nb$_{0.2}$O$_7$ and 7*M* Ca$_2$Ta$_{1.9}$Nb$_{0.1}$O$_7$ are approximately stable (18–19) from 100 kHz up to 5 GHz and reach a maximum (22, 24.5 and 26.1, respectively) at ∼ 8 GHz. The dielectric constant is comparable for some important microwave dielectrics, such as BaMg$_{1/3}$Ta$_{2/3}$O$_3$ (∼ 24; Reaney & Iddles, 2006). However, the problem with these systems is that they have low quality factors ($Q \simeq 200$) for technical applications (Grey *et al.*, 2001).

It is interesting to see that 8*O* Ca$_2$Ta$_2$O$_7$, which is synthesized by the optical floating zone melting method from 3*T* Ca$_2$Ta$_2$O$_7$ powder, has a relatively high dielectric constant (∼ 60) at room temperature (Ebbinghaus *et al.*, 2005). And ε_r increases to 90 at 50 K. The high dielectric constant may result from a net dipole created by the off-center Ta^{5+} in the TaO$_6$ octahedra of the Ca$_3$Ta layers. The shifting of Ta^{5+} also produces two short Ta—O bonds and two long Ta—O bonds, leading to the distortion of TaO$_6$ octahedra. The high dielectric constant and the ability to tailor it are interesting for scientific study and possible electronic applications.

In addition, the crystallographic study of Nd$_2$Zr$_2$O$_7$ and Sm$_2$Ti$_2$O$_7$ doping Ca$_2$Ta$_2$O$_7$ has been conducted by Grey *et al.* (Grey *et al.*, 2003; Grey & Roth, 2000). The resulting phases include 3*T*, 4*M*, 5*M* and 6*T* weberites. The great structural flexibility of Ca$_2$Ta$_2$O$_7$-based compounds is interesting in a crystallographic study and may have potentials in technical applications.

3.2.2. Weberite-type Ln$_3$NbO$_7$. As stated in §2.3, Ln$_2$(Nb,Ln)O$_7$ (or Ln$_3$NbO$_7$, where Ln is La^{3+}, Pr^{3+}, Nd^{3+} and Gd^{3+}) is a weberite-type structure. It is an extreme case of 2*O*-

III weberite structure, in which *A*-2 and *B*-2 are the same. Our recent study on the dielectric properties of Ln$_3$NbO$_7$ (Ln = La^{3+}, Nd^{3+} and Gd^{3+}) showed some interesting results (Cai *et al.*, 2007; Cai & Nino, 2007). As shown in Fig. 15, all three compounds exhibited a dielectric relaxation behavior similar to that observed in pyrochlore compounds (Roth *et al.*, 2008; Nino *et al.*, 2001). The permittivity increases sharply with increasing temperature until a maximum is reached. After that, the permittivity decreases slightly with an increase in temperature. The permittivity is between 35 and 60 for La$_3$NbO$_7$ and 34–47 for Gd$_3$NbO$_7$ from 113 to 473 K, and is between 34 and 62 for Nd$_3$NbO$_7$ from 113 to 673 K at 1 MHz. These three compounds have close permittivity at 113 K. The relaxation temperatures are different, 183, 473 and 323 K for La$_3$NbO$_7$, Nd$_3$NbO$_7$ and Gd$_3$NbO$_7$, respectively. The difference in relaxation temperature indicates the possibility of tailoring the temperature at which dielectric relaxation occurs through variations in compositions. As for the origin of different dielectric relaxation temperatures, a possible explanation is provided by comparing the structure. The main difference between the structure is that in Gd$_3$NbO$_7$ the polyhedra are more distorted (Wakeshima *et al.*, 2004; Allpress & Rossell, 1979; Rossell, 1979). In Table 8 polyhedral distortions are quantified in the deviation of bond length and bond angle. The calculation is based on the atomic positions after Rossell (1979). Nd$_3$NbO$_7$ has nearly perfect NbO$_6$ octahedra, while Gd$_3$NbO$_7$ has the most distorted octahedra. The LnO$_8$ cube in Nd$_3$NbO$_7$ is the least distorted while LaO$_8$ and GdO$_8$ cubes have comparable distortion. These distortions are attributed to the 'openness' of the structure which causes an easier polarization of the material and results in a lower relaxation temperature (Astafyev *et al.*, 1985). Additional details on the relationship of dielectric relaxation and polyhedral distortions are ongoing and will be a matter for future publications.

Owing to the interesting dielectric loss behavior observed in Gd$_3$NbO$_7$ its characterization includes more frequencies (1, 4, 6, 10, 30, 80, 100, 300, 800 kHz and 1 MHz), as shown in Fig. 15(*c*). The temperature (T_m), at which the loss peak occurs increases with increasing measuring frequency. To better understand the phenomena, the Arrhenius function is used to model the relaxation behaviour of Gd$_3$NbO$_7$

$$ \nu = \nu_0 \exp\left(-\frac{E_a}{k_B T_m}\right), \tag{5} $$

where ν is the measuring frequency, the pre-exponential ν_0 is the attempt-jump frequency, E_a is the activation energy and k_B is Boltzmann's constant. T_m is determined for each measuring frequency by fitting the loss peak to a Gaussian function. The non-symmetric tails of loss peaks are cut off during fitting. The resulting Arrhenius plot is presented in Fig. 15(*d*). From the linear fit, $\nu_0 = 1.51 \times 10^{11}$ Hz, and the activation energy E_a is 0.45 eV, which is larger than typical values observed in Nb-based pyrochlores, for example 0.32 eV in Ca–Ti–Nb–O pyrochlore and 0.14 eV in Bi–Zn–Nb–O pyrochlore (Roth *et al.*, 2008; Nino, 2002). However, other ionic and dipolar compounds systems have even higher activation energies; for

example, 0.53 eV for CaF_2-doped NaF and 1.02 eV for $(Ba_{0.8}Sr_{0.2})(Ti_{1-x}Zr_x)O_3$ (Johnson *et al.*, 1969; Cheng *et al.*, 2004). Thus, the calculated E_a is acceptable.

The dielectric study of Ln_3NbO_7 compounds points to the possibility of tailoring the dielectric relaxation and develop further a paradigm for the compositional design of fluorite-related ceramics with optimized dielectric properties.

4. Conclusions

There are a considerable number of weberite compounds $(A_2B_2X_7)$ that have been studied to date. Here the stability field in terms of the ratio of R_A and R_B, and the relative bond ionicity has been established. This structure can be interpreted in different ways. As an anion-deficient fluorite structure, it has similar close-packed cationic networks as fluorite and pyrochlore. It is presented here that the cation sublattices of the weberite and the pyrochlore structures are correlated by an axial transformation and that the different stacking inside

an AB_3 and A_3B cation slab leads to a different coordination environment of anions in weberite and pyrochlore. There are various types of weberite-like structures. They can be distinguished by the number of AB_3 and A_3B slabs and the crystal system. B chains are a characteristic of all weberite structures even for weberite polytypes with $N > 4$. The stacking sequence and the orientation of B-chains changes with respect to monoclinic and trigonal variants.

So far, investigations have primarily focused on the crystallographic aspects of weberites and some weberite compounds are reported to have interesting properties. It is clear that they are of great scientific interest. However, few studies have concentrated on the properties and possible applications. There is no doubt that weberite compounds possess various useful properties that can be tailored owing to the fact that many metal cations can be introduced into this structure as well as that a large diversity of variants exist in this structure. The realisation of the potential of weberites for electrical applications will grow as more extensive studies are conducted and knowledge of the structures increases.
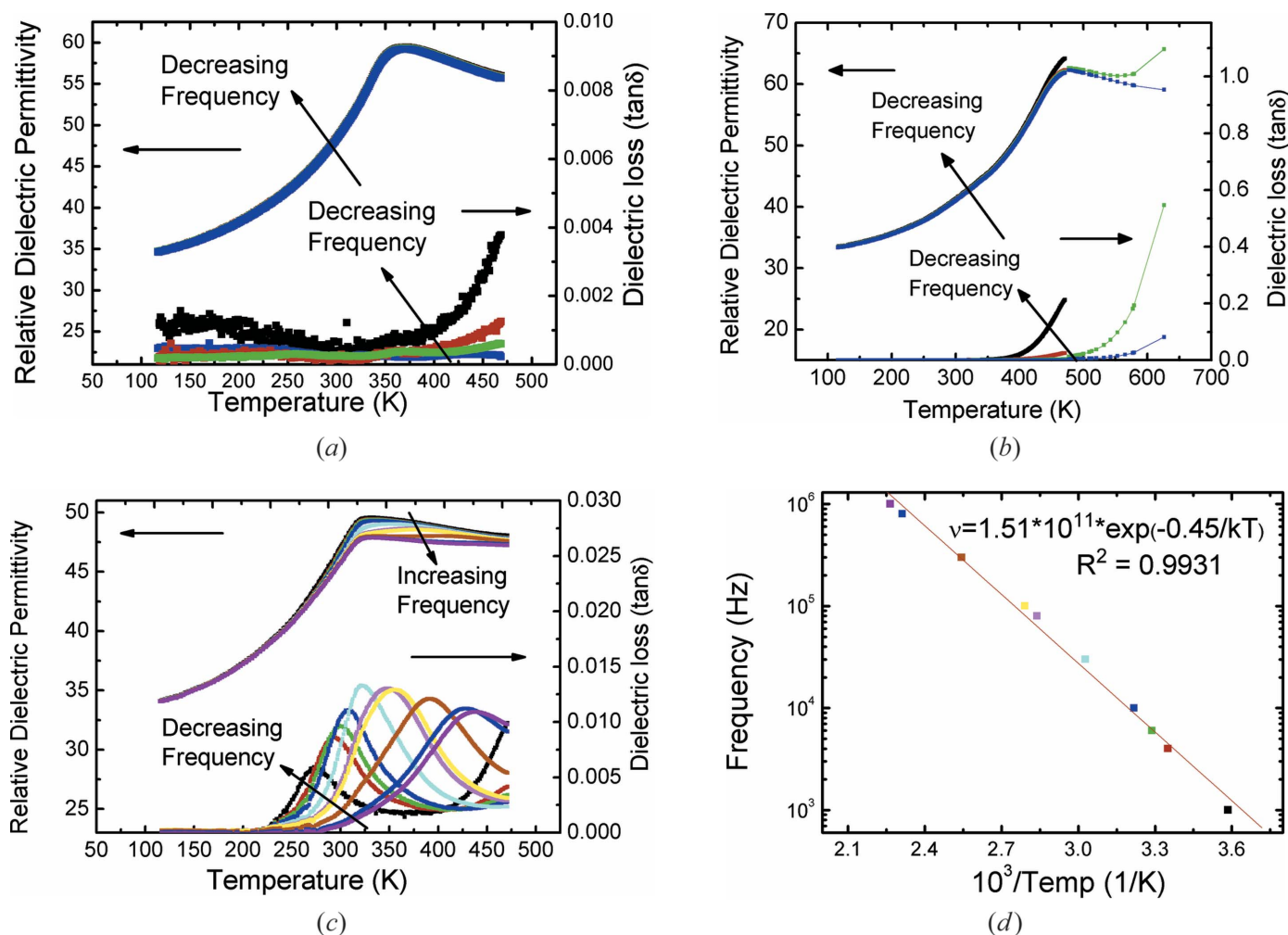

Figure 15
Dielectric properties between 1 kHz and 1 MHz of (a) La_3NbO_7, (b) Nd_3NbO_7, (c) Gd_3NbO_7 and (d) Arrhenius analysis of Gd_3NbO_7.

References

Abe, R., Higashi, M., Sayama, K., Abe, Y. & Sugihara, H. (2006). *J. Phys. Chem. B*, **110**, 2219–2226.

Abe, R., Higashi, M., Zou, Z. G., Sayama, K., Abe, Y. & Arakawa, H. (2004). *J. Phys. Chem. B*, **108**, 811–814.

Aia, M. A., Mooney, R. W. & Hoffman, C. W. W. (1963). *J. Electrochem. Soc.* **110**, 1048–1054.

Aleshin, E. & Roy, R. (1962). *J. Am. Ceram. Soc.* **45**, 18–25.

Allpress, J. G. & Rossell, H. J. (1979). *J. Solid State Chem.* **27**, 105–114.

Allred, A. L. & Rochow, E. G. (1958). *J. Inorg. Nucl. Chem.* **5**, 264–268.

Astafev, A. V., Bush, A. A., Stefanovich, S. Y. & Venevtsev, Y. N. (1985). *Inorg. Mater.* **21**, 560–563.

Astafyev, A. V., Sirotinkin, V. P. & Stefanovich, S. Y. (1985). *Kristallografiya*, **30**, 603–604.

Au, Y. S., Fu, W. T. & Ijdo, D. J. W. (2007). *J. Solid State Chem.* **180**, 3166–3171.

Barrier, N. & Gougeon, P. (2003). *Acta Cryst.* E**59**, i22–i24.

Batanov, S. S. (1975). *Zh. Neorg. Khim.* **20**, 2595–2600.

Bayliss, P., Mazzi, F., Munno, R. & White, T. J. (1989). *Mineral. Mag.* **53**, 565–569.

Bogvad, R. (1938). *Meddelelser om Grønland*, **119**, 1–11.

Boireau, A., Gravereau, P., Dance, J. M., Tressaud, A., Hagenmuller, P., Soubeyroux, J. L., Welsch, M. & Babel, D. (1993). *Mater. Res. Bull.* **28**, 27–38.

Bonazzi, P. & Bindi, L. (2007). *Am. Mineral.* **92**, 947–953.

Bontchev, R. P., Jacobson, A. J., Gospodinov, M. M., Skumryev, V., Popov, V. N., Lorenz, B., Meng, R. L., Litvinchuk, A. P. & Iliev, M. N. (2000). *Phys. Rev. B*, **62**, 12235–12240.

Brese, N. E. & O'Keeffe, M. (1991). *Acta Cryst.* B**47**, 192–197.

Brisse, F., Stewart, D. J., Seidl, V. & Knop, O. (1972). *Can. J. Chem.* **50**, 3648.

Brown, D. I. (2002). *The Chemical Bond in Inorganic Chemistry: The Bond Valence Model.* Oxford University Press.

Burchard, G. & Rudorff, W. (1979). *Z. Anorg. Allg. Chem.* **454**, 107–112.

Butler, K. H., Bergin, M. J. & Hannaford, V. M. B. (1950). *J. Electrochem. Soc.* **97**, 117–122.

Byström, A. (1944). *Ark. Kemi Miner. Och Geol. B*, **18**, 1–7.

Bystrom, A. (1945). *Ark. Kemi Miner. Och Geol. A*, **18**, 1–8.

Cai, L., Guzman, J., Perez, L. & Nino, J. C. (2007). *Solid-State Chemistry of Inorganic Materials VI*, Materials Research Society Symposium Proceeding, 998E, 0988-qq0901-0904.

Cai, L. & Nino, J. C. (2007). *J. Eur. Ceram. Soc.* **27**, 3971–3976.

Caramanian, A., Souron, J. P., Gredin, P. & de Kozak, A. (2001). *J. Solid State Chem.* **159**, 234–238.

Cava, R. J., Krajewski, J. J. & Roth, R. S. (1998). *Mater. Res. Bull.* **33**, 527–532.

Chassain, J. (1969). *C. R. Hebd. Seances Acad. Sci. C*, **268**, 2188.

Cheng, B. L., Wang, C., Wang, S. Y., Button, T. W., Lu, H. B., Zhou, Y. L., Chen, Z. H. & Yang, G. Z. (2004). *Appl. Phys. Lett.* **84**, 5431–5433.

Coelho, A. A., Cheary, R. W. & Smith, K. L. (1997). *J. Solid State Chem.* **129**, 346–359.

Cordfunke, E. H. P. & Ijdo, D. J. W. (1988). *J. Phys. Chem. Solids*, **49**, 551–554.

Cosier, R., Wise, A., Tressaud, A., Grannec, J., Olazcuag, R. & Portier, J. (1970). *C. R. Hebd. Seances Acad. Sci. C*, **271**, 142–145.

Courbion, G., Ferey, G., Holler, H. & Babel, D. (1988). *Eur. J. Solid State Inorg. Chem.* **25**, 435–447.

Dahlke, P. & Babel, D. (1994). *Z. Anorg. Allg. Chem.* **620**, 1692–1697.

Dahlke, P., Peschel, B. & Babel, D. (1998). *Z. Anorg. Allg. Chem.* **624**, 1003–1010.

Dance, J. M., Grannec, J., Jacoboni, C. & Tressaud, A. (1974). *C. R. Hebd. Seances Acad. Sci. C*, **279**, 601–604.

Desgardin, G., Robert, C. & Raveau, B. (1976). *Can. J. Chem.* **54**, 1665–1671.

Desgardin, G., Robert, C. & Raveau, B. (1977). *J. Inorg. Nucl. Chem.* **39**, 907–908.

Ebbinghaus, S. G., Kalytta, A., Kopf, J., Weidenkaff, A. & Reller, A. (2005). *Z. Kristallogr.* **220**, 269–276.

Frenzen, G., Massa, W., Babel, D., Ruchaud, N., Grannec, J., Tressaud, A. & Hagenmuller, P. (1992). *J. Solid State Chem.* **98**, 121–127.

Gade, K. & Chincholkar, V. S. (1979). *J. Chem. Soc. Dalton Trans.* p. 1959.

Gemmill, W. R., Smith, M. D. & zur Loye, H. C. (2004). *Inorg. Chem.* **43**, 4254–4261.

Gemmill, W. R., Smith, M. D. & zur Loye, H. C. (2007). *J. Chem. Cryst.* **37**, 793–795.

Gemmill, W. R., Smith, M. D., Mozharivsky, Y. A., Miller, G. J. & zur Loye, H. C. (2005). *Inorg. Chem.* **44**, 7047–7055.

Giuseppetti, G. & Tadini, C. (1978). *Tschermaks Min. Petr. Mitt.* **25**, 57–62.

Gravereau, P., Boireau, A., Dance, J. M., Trut, L. & Tressaud, A. (1992). *Acta Cryst.* C**48**, 2108–2111.

Greedan, J. E., Raju, N. P., Wegner, A., Gougeon, P. & Padiou, J. (1997). *J. Solid State Chem.* **129**, 320–327.

Greneche, J. M., Linares, J., Varret, F., Laligant, Y. & Ferey, G. (1988). *J. Magn. Magn. Mater.* **73**, 115–122.

Grey, I. E., Mumme, W. G., Ness, T. J., Roth, R. S. & Smith, K. L. (2003). *J. Solid State Chem.* **174**, 285–295.

Grey, I. E. & Roth, R. S. (2000). *J. Solid State Chem.* **150**, 167–177.

Grey, I. E., Roth, R. S., Mumme, G., Bendersky, L. & Minor, D. (1999). *Solid State Chemistry of Inorganic Materials II*, Materials Research Society Symposium Proceedings, Vol. 547, pp. 127–138. Boston, MA: Materials Research Society.

Grey, I. E., Roth, R. S., Mumme, W. G., Planes, J., Bendersky, L., Li, C. & Chenavas, J. (2001). *J. Solid State Chem.* **161**, 274–287.

Groen, W. A. & IJdo, D. J. W. (1988). *Acta Cryst.* C**44**, 782–784.

Groen, W. A., van Berkel, F. P. F. & IJdo, D. J. W. (1987). *Acta Cryst.* C**43**, 2262–2264.

Haegele, R., Verscharen, W., Babel, D., Dance, J. M. & Tressaud, A. (1978). *J. Solid State Chem.* **24**, 77–84.

Hall, W., Kim, S., Zubieta, J., Walton, E. G. & Brown, D. B. (1977). *Inorg. Chem.* **16**, 1884–1887.

Hansler, R. & Rudorff, W. (1970). *Z. Naturforsch. B*, **25**, 1306.

Harada, D. & Hinatsu, Y. (2001). *J. Solid State Chem.* **158**, 245–253.

Harada, D. & Hinatsu, Y. (2002). *J. Solid State Chem.* **164**, 163–168.

Harada, D., Hinatsu, Y. & Ishii, Y. (2001). *J. Phys. Condens. Matter*, **13**, 10825–10836.

Heger, G. (1973). *Int. J. Magn.* **5**, 119–124.

Hinatsu, Y., Wakeshima, M., Kawabuchi, N. & Taira, N. (2004). *J. Alloys Compd*, **374**, 79–83.

Isupov, V. A. (2000). *Ferroelectr. Rev.* **2**, 115–168.

Ivanov, S., Tellgren, R. & Rundlof, H. (1998). European Powder Diffraction Conference 5, Pts 1 and 2 278–2, pp. 768–772.

Ivanov, S. A. & Zavodnik, V. E. (1990). *Kristallografiya*, **35**, 842–846.

Johnson, H. B., Tolar, N. J., Miller, G. R. & Cutler, I. B. (1969). *J. Phys. Chem. Solids*, **30**, 31–42.

Kahnharari, A., Mazerolles, L., Michel, D. & Robert, F. (1995). *J. Solid State Chem.* **116**, 103–106.

Khalifah, P., Erwin, R. W., Lynn, J. W., Huang, Q., Batlogg, B. & Cava, R. J. (1999). *Phys. Rev. B*, **60**, 9573–9578.

Khalifah, P., Huang, Q., Lynn, J. W., Erwin, R. W. & Cava, R. J. (2000). *Mater. Res. Bull.* **35**, 1–7.

Klein, W., Curda, J., Peters, E. M. & Jansen, M. (2006). *Z. Anorg. Allg. Chem.* **632**, 1508–1513.

Knop, O., Cameron, T. S. & Jochem, K. (1982). *J. Solid State Chem.* **43**, 213–221.

feature articles

Knop, O. & Demazeau, G. (1981). *J. Solid State Chem.* **39**, 94–99.

Knop, O., Demazeau, G. & Hagenmuller, P. (1980). *Can. J. Chem. Rev.* **58**, 2221–2224.

Koch, J. & Hebecker, C. (1985). *Naturwissenschaften*, **72**, 431–432.

Koch, J. & Hebecker, C. (1988). *Naturwissenschaften*, **75**, 360.

Koch, J., Hebecker, C. & John, H. (1982). *Z. Naturforsch. B*, **37**, 1659–1660.

Kummer, S., Massa, W. & Babel, D. (1988). *Z. Naturforsch. B*, **43**, 694–701.

Laligant, Y., Calage, Y., Heger, G., Pannetier, J. & Ferey, G. (1989). *J. Solid State Chem.* **78**, 66–77.

Laligant, Y., Calage, Y., Torrestapia, E., Greneche, J. M., Varret, F. & Ferey, G. (1986). *J. Magn. Magn. Mater.* **61**, 283–290.

Laligant, Y., Ferey, G., Heger, G. & Pannetier, J. (1987). *Z. Anorg. Allg. Chem.* **553**, 163–171.

Laligant, Y., Leblanc, M., Pannetier, J. & Ferey, G. (1986). *J. Phys. C*, **19**, 1081–1095.

Laligant, Y., Pannetier, J., Labbe, P. & Ferey, G. (1986). *J. Solid State Chem.* **62**, 274–277.

Laligant, Y., Pannetier, J., Leblanc, M., Labbe, P., Heger, G. & Ferey, G. (1987). *Z. Kristallogr.* **181**, 1–10.

Lam, R., Langet, T. & Greedan, J. E. (2003). *J. Solid State Chem.* **171**, 317–323.

Lam, R., Wiss, F. & Greedan, J. E. (2002). *J. Solid State Chem.* **167**, 182–187.

Leroux, F., Mar, A., Guyomard, D. & Piffard, Y. (1995). *C. R. Acad. Sci.* **320**, 147–153.

Lin, X. P., Huang, F. Q., Wang, W. D., Wang, Y. M., Xia, Y. J. & Shi, J. L. (2006). *Appl. Catal. Gen.* **313**, 218–223.

Little, E. J. & Jones, M. M. (1960). *J. Chem. Educ.* **37**, 231–233.

Lopatin, S. S., Averyanova, L. N. & Belyaev, I. N. (1985). *Zh. Neorg. Khim.* **30**, 867–872.

Lopatin, S. S., Averyanova, L. N., Belyaev, I. N., Zvyagintsev, B. I. & Dyatlov, E. V. (1982). *Zh. Neorg. Khim.* **27**, 2751–2755.

Mekata, M. (2003). *Phys. Today*, **56**, 12–13.

Milyan, P. M. & Semrad, E. E. (2005). *Russ. J. Inorg. Chem.* **50**, 1599–1604.

Nino, J. C. (2002). PhD dissertation. The Pennsylvania State University.

Nino, J. C., Lanagan, M. T. & Randall, C. A. (2001). *J. Appl. Phys.* **89**, 4512–4516.

Nishimine, H., Doi, Y., Hinatsu, Y. & Sato, M. (2007). *J. Ceram. Soc. Jpn*, **115**, 577–581.

Nishimine, H., Wakeshima, M. & Hinatsu, Y. (2004). *J. Solid State Chem.* **177**, 739–744.

Nishimine, H., Wakeshima, M. & Hinatsu, Y. (2005). *J. Solid State Chem.* **178**, 1221–1229.

Pankhurst, Q. A., Johnson, C. E. & Wanklyn, B. M. (1991). *J. Magn. Magn. Mater.* **97**, 126–130.

Peschel, B. & Babel, D. (1997). *Z. Anorg. Allg. Chem.* **623**, 1614–1620.

Peschel, B., Molinier, M. & Babel, D. (1995). *Z. Anorg. Allg. Chem.* **621**, 1573–1581.

Plaisier, J. R., Drost, R. J. & IJdo, D. J. W. (2002). *J. Solid State Chem.* **169**, 189–198.

Reading, J., Knee, C. S. & Weller, M. T. (2002). *J. Mater. Chem.* **12**, 2376–2382.

Reaney, I. M. & Iddles, D. (2006). *J. Am. Ceram. Soc.* **89**, 2063–2072.

Renaudin, J., Leblanc, M., Ferey, G., Dekozak, A. & Samouel, M. (1988). *J. Solid State Chem.* **73**, 603–609.

Rooksby, H. P. & White, E. A. D. (1964). *J. Am. Ceram. Soc.* **47**, 94–96.

Rossell, H. J. (1979). *J. Solid State Chem.* **27**, 115–122.

Roth, R. S., Vanderah, T. A., Bordet, P., Grey, I. E., Mumme, W. G., Cai, L. & Nino, J. C. (2008). *J. Solid State Chem.* **181**, 406–414.

Ruchaud, N., Grannec, J., Gravereau, P., Nunez, P., Tressaud, A., Massa, W., Frenzen, G. & Babel, D. (1992). *Z. Anorg. Allg. Chem.* **610**, 67–74.

Sato, J., Saito, N., Nishiyama, H. & Inoue, Y. (2002). *J. Photochem. Photobiol. A*, **148**, 85–89.

Schmidt, R. E., Massa, W. & Babel, D. (1992). *Z. Anorg. Allg. Chem.* **615**, 11–15.

Scott, H. G. (1990). *Z. Kristallogr.* **190**, 41–46.

Shannon, R. D. (1976). *Acta Cryst.* A**32**, 751–767.

Subramanian, M. A., Aravamudan, G. & Rao, G. V. S. (1983). *Prog. Solid State Chem.* **15**, 55–143.

Subramanian, M. A., Marshall, W. J., Hoffmann, R. D. & Sleight, A. W. (2006). *Z. Naturforsch. B*, **61**, 808–812.

Sych, A. M., Kabanova, M. I. & Andreeva, S. G. (1988). *Zh. Neorg. Khim.* **33**, 2756–2760.

Sych, A. M., Kabanova, M. I., Garbuz, V. V. & Kovalenko, E. N. (1988). *Inorg. Mater.* **24**, 1316–1320.

Syozi, I. (1951). *Prog. Theor. Phys.* **6**, 306–308.

Thompson, G. R., Pankhurst, Q. A. & Johnson, C. E. (1992). *J. Magn. Magn. Mater.* **104**, 893–894.

Tressaud, A., Dance, J. M., Portier, J. & Hagenmul, P. (1974). *Mater. Res. Bull.* **9**, 1219–1226.

Vanberkel, F. P. F. & Ijdo, D. J. W. (1986). *Mater. Res. Bull.* **21**, 1103–1106.

Vente, J. F., Helmholdt, R. B. & Ijdo, D. J. W. (1994). *J. Solid State Chem.* **108**, 18–23.

Vente, J. F. & Ijdo, D. J. W. (1991). *Mater. Res. Bull.* **26**, 1255–1262.

Verscharen, W. & Babel, D. (1978). *J. Solid State Chem.* **24**, 405–421.

Wakeshima, M. & Hinatsu, Y. (2006). *J. Solid State Chem.* **179**, 3575–3581.

Wakeshima, M., Nishimine, H. & Hinatsu, Y. (2004). *J. Phys. Condens. Matter*, **16**, 4103–4120.

Weil, M. & Werner, F. (2001). *Monatsh. Chem.* **132**, 769–777.

Weller, M. T., Reading, J. & Knee, C. S. (2003). *Solid State Chem.* **90–91**, 201–205.

Welsch, M. & Babel, D. (1992). *Z. Naturforsch. B*, **47**, 685–692.

White, T. J. (1984). *Am. Mineral.* **69**, 1156–1172.

Wiss, F., Raju, N. P., Wills, A. S. & Greedan, J. E. (2000). *Int. J. Inorg. Mater.* **2**, 53–59.

Wltschek, G., Paulus, H., Svoboda, I., Ehrenberg, H. & Fuess, H. (1996). *J. Solid State Chem.* **125**, 1–4.

Wyckoff, R. W. G. (1963). *Crystal Structures.* New York: Interscience Publishers.

Yakubovich, O., Urusov, V., Massa, W., Frenzen, G. & Babel, D. (1993). *Z. Anorg. Allg. Chem.* **619**, 1909–1919.

Yakubovich, O. V., Urusov, V. S., Frenzen, G., Massa, W. & Babel, D. (1990). *Eur. J. Solid State Inorg. Chem.* **27**, 467–475.

290   Lu Cai and Juan C. Nino · Complex Ceramic Structures. I

Acta Cryst. (2009). B**65**, 269–290